Applied Catalysis B: Environmental 156–157 (2014) 213–235

Contents lists available at ScienceDirect

Applied Catalysis B: Environmental

journal homepage: www.elsevier.com/locate/apcatb

Review

Decahedral TiO_2 with exposed facets: Synthesis, properties, photoactivity and applications

Ewelina Grabowska*, Magdalena Diak, Martyna Marchelek, Adriana Zaleska

Department of Environmental Technology, Faculty of Chemistry, University of Gdansk, Wita Stwosza 63, PL80-952 Gdansk, Po

ARTICLE INFO

Article history:
Received 3 December 2013
Received in revised form 5 March 2014
Accepted 11 March 2014
Available online 20 March 2014

Keywords:
titanium dioxide
crystals facets
high reactive (0 0 1) facets
synthesis
properties
applications

ABSTRACT

As an important metal oxide, titanium diox[i]been widely [i]ated because of its unique surface, electronic, and photocatalytic properties which [m]e this mater[i]applicable in many areas of science and technology ranging from adsorption, catalysis and photocatalysis to biomedicine, environmental monitoring and cleanup, energy c[o]ion and stora[g]c. The properties of anatase TiO_2 crystals are largely determined by external [f]aces exposed. Since [t]e breakthrough in synthesizing anatase TiO_2 single crystals with a large p[e]ntage of highly reactive (0 0 1) facets in 2008, many unusual properties and applications of these (0 0 1) facets d[o]inant in anatase TiO_2 have been explored theoretically and experimentally, showing [i]ndustrial i[m]rtance of this semiconductor material. Here we review the recent progress in synthesi[s] by vario[u]ynthetic methods and photocatalytic activity TiO_2 with exposed crystal f[a]with differe[n]ogies.

Contents

1. Introduction

Semic[o]uctor [p]rticles a[r]tractive materials photocatalysts becau[s]the l[a]number of surface reaction sites, and semiconducto[r] [p]rticles [w]rge surface area have been utilized for various kin[d]f photocatalytic reaction, such as organic decomposition and [w]r splitting [1–7]. As one of the most important photocatalysts, [T]$_2$-based materials have demonstrated a great potential in many applications, including water splitting to generate O_2 and H_2 [8–15], a sustainable process for treatment of water and wastewater [16–18], gas phase treatment [19–23] as well as in solar cells [24–28] and self-cleaning surfaces [29–33].

According to the Wulff construction, the equilibrium shape of an anatase crystal is a slightly truncated tetragonalbipyramid enclosed by eight (1 0 1) facets and two (0 0 1) facets, with the most stable (1 0 1) facets accounting for 94% of the total surface (Fig. 1) [34]. Based on the photo-oxidation reaction results, it was stated that the sharp TiO_2 anatase nanocrystals with a long distance in the (0 0 1) direction ($d_{(001)}$) has a high photocatalytic activity. Moreover, it has been reported that titanium (IV) oxide (TiO_2) particles with specific exposed crystal faces, i.e., decahedral anatase with (1 0 1) and (0 0 1) exposed crystal faces and dodecahedral rutile with (1 1 0) and (1 0 1) exposed crystal faces, showed excellent photocatalytic activity despite the large particle size (~1 μm) [35–39]. Murakami et al. indicated that different energy levels of conduction and valence bands, which are determined by the arrangement and kind of constituent atoms, drive the electrons and positive holes to different exposed crystal faces, resulting in a decrease in the back-reaction rate by predominant progress of reduction and

* Corresponding author. Tel.: +48 58 523 52 22.
E-mail address: ewelina.grabowska@ug.edu.pl (E. Grabowska).

http://dx.doi.org/10.1016/j.apcatb.2014.03.019
0926-3373/

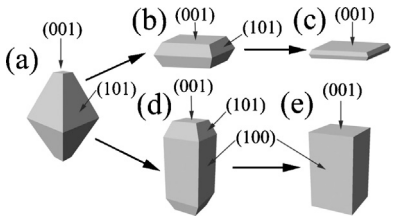

Fig. 1. Schematic drawings of anatase shapes: (a) slightly truncated tetragonal bipyramid with dominant (1 0 1) facets (equilibrium crystal shape); (b) truncated tetragonal bipyramid with a large percentage of top (0 0 1) facets; (c) square sheet with dominant (0 0 1) facets; (d) elongated truncated tetragonal bipyramid with a large percentage of lateral (1 0 0) facets; (e) tetragonal cuboid enclosed by (1 0 0) and (0 0 1) facets. Reprinted from ref. [34].

oxidation on each crystal face [40]. It was shown that optical, magnetic, dielectric, and chemical properties of a particle are depend on the shape of the crystal particle [41,42], while an electrode experiment using single-crystal rutile TiO_2 has indicated that photoelectrochemical properties also depend on the kind of exposed crystal face [43,44]. The results of those studies suggest that it is possible to optimize activity of a specific photocatalytic reaction by controlling the kind and surface area of the exposed crystal face on semiconductor particles [40].

Design and morphological control of crystal facets is a commonly employed strategy to optimize the performance of various crystalline catalysts from noble metals to semiconductors [39,45,46]. The basis of this strategy is that surface atomic configuration and coordination, which inherently determine their heterogeneous photoreactivity, can be finely tuned by morphological control. The conventional understanding of the surface atomic structure of a crystal is that facets with a higher percenta undercoordinated atoms are usually more reactive in heter neous reactions. For instance (0 0 1) facets of anatase TiO_2 considered to be more reactive than (1 0 1) [39].

The key to controlling the percentage of crystal facets of anatase crystals is to change the relative sta y of facet during crystal growth, which is intrinsicall termi by the surface energies of the facets. Surface a orb are known to be very effective in cha g the s e energy of TiO_2 facets and thus the percenta facets [39]. lts have shown that the percentage of (0 f anatase c tals can be increased from 18 up to about 90%, de ing on the different synthesis routes. These res indicate that r facets such as (0 1 0), the surface energ which (0.53 J m^{-2}) between those of (1 0 1) (0.44 J m^{-2}) a 0 0 1) J m^{-2}) [47,48], might also be acquired by fine-tuning p meters i a given synthesis route so that a favorable surface rgy for wing such facets can be obtained. Wh e-ads f ine atoms are used as the morphologi contr g agen an facets are easily obtained by simpl ination [39].

Decahed i coa btained by three main approaches: (1) hydrother olvothermal route [38,40,49–58], (2) hydrolysis of TiO_2 precu in ethylene glycol [59], or (3) by gas phase reaction [37,60], as ematically shown in Fig. 2. Importantly, all hydrothermal/solvothermal synthesis routes, reported to prepare anatase TiO_2 crystals with high-energy facets, used F^-containing compounds as capping agents to control the morphology, which is quite toxic and corrosive. Thus, it is highly desirable to develop a new synthesis strategy with reduced or no fluorine containing compounds as capping agents. More importantly, organic surfactants adsorbing onto the surfaces can also remarkably change the free energy of these surfaces and interfacial properties, but the choice of surfactant remains empirical due to many unsolved issues including a quantitative description of the adsorption behavior and in-depth understanding of selective surface-adsorption energies on nanocrystals.

Considering so many breakthroughs have been reported and the fast advances in the preparation of TiO_2 with exposed facets in the past few years, we believe that a comprehensive review of this important functional material will further promote the research in this field. Moreover the attention will concentrate on the mechanisms of shape evaluation of TiO_2, photocatalytic activity of different sites of TiO_2 facets and applications of TiO_2 dominated with highly reactive facets.

2. Mechanism of shape evolution of TiO_2

The energy of the terminated surface of a solid material is always higher than that of the bulk and this en ence is defined as the surface energy. Based on surfa energies l facets, one can use the Wulff construction to d ine the eq brium morphology of a material. In the W ff c uction, s ace energy minimization is the central s dard to o ize t composition of the crystal surface [61].

The truncated octah bipy id, havin ght (1 0 1) facets and two (0 0 1) face , is a popular ystal shape observed in nature and the st com shape anatase crystals based on Wulff constr on [62,63]. size anatase TiO_2 crystals with domina g ergy (0 0 1) ts, the crystal growth should to be confine with a kinetically controlled regime under non equilibri m conditions [48].

M i et al. propos plausible mechanism of shape evolution of anatase particles in the presence of polyvinyl alcohol (PVA) (F 3a):

(1) f tion natase rods having stacked structure with decahedr ase with (1 0 1) and (0 0 1) crystal faces and growth in the (0 0 1) direction;
(2) ormation of anatase rods into octahedral anatase by size reduction along the (0 0 1) direction or by being split along the (0 0 1) plane in the dissolution process;
(3) growth of anatase particle in the (0 0 1) direction with exposure of the (1 0 1) crystal face and evolution of decahedral anatase with large $d_{A(004)}$ in the recrystallization process [40].

Murakami et al. stated that the presence of PVA prevented the nucleation of rutile phase. Moreover, fine particles with a narrow size distribution that were prepared under an acidic condition, suggest that PVA may lead a prevention of aggregation and a formation of a flat exposed surface by adsorption on TiO_2 in the crystallization process [40].

The mechanism of anatase TiO_2 single crystals formation with 27–50% reactive (0 0 1) facets *via* a microwave-enhanced ionothermal method was explained by Zhang et al. (Fig. 3b) [64]. An aqueous solution of titanium tetrafluoride and ionic liquid (1-methylimidazolium tetrafluoroborate) were involved during preparation procedure. In the microwave frequency range, polar molecules, such as H_2O, orientate with the electric field. When dipolar molecules reorientate with respect to an alternating electric field, they lose energy in the form of heat by molecular friction. The ability of the solvent to heat in the microwave field is dependent on the dielectric loss constant. Because water has high dielectric losses it is an ideal solvent for microwave rapid heating. The ionic liquid in this reaction system provides a synergistic effect to absorb the microwaves. This may explain why this method is efficient in the synthesis of anatase single-crystals [64]. A control experiment by using conventional hydrothermal conditions shows that at least 48 h were required for the synthesis of TiO_2 single-crystals exposed with (0 0 1) facets. The SEM image confirmed that anatase TiO_2 single-crystals are highly aggregated sheets. These results indicate that microwaves can provide rapid and uniform heating of reagent and solvents. Fast heating accelerates the hydrolysis of TiF_4 and

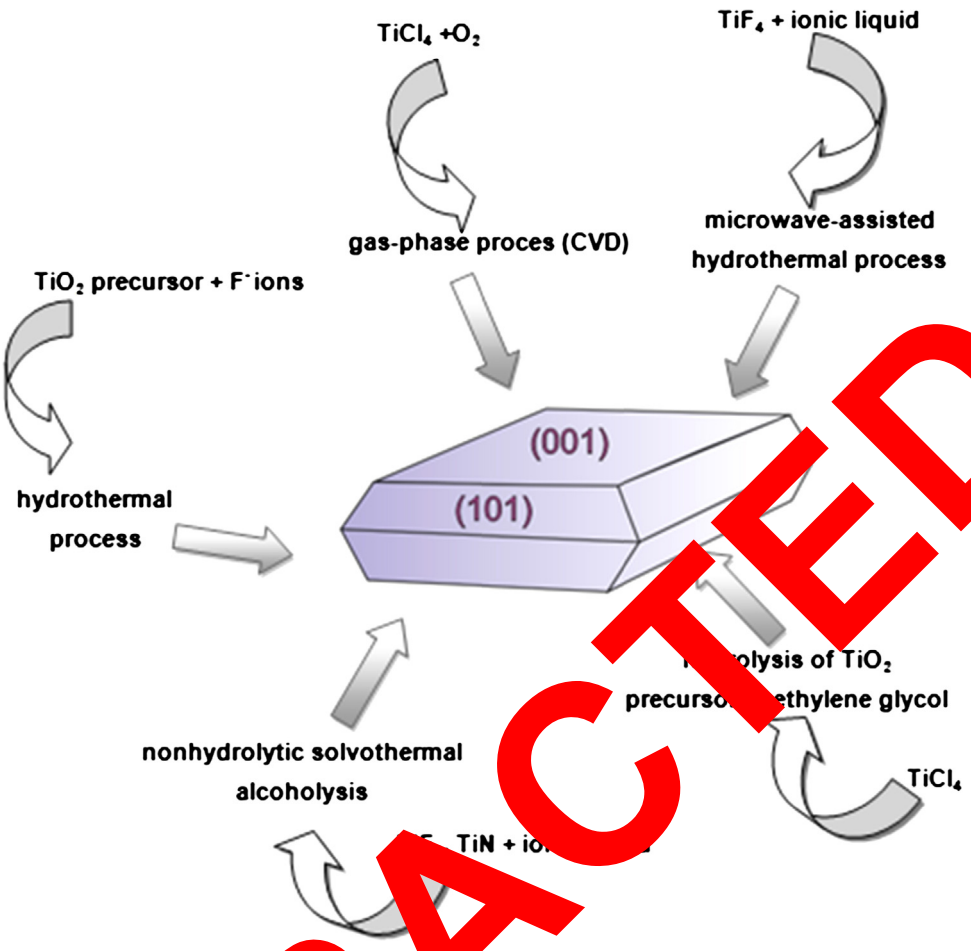

ble prep on routes of decahedral TiO_2.

nucleation of the anatase cluster. The ho eneou icrowav heating also provides uniform nucleation a s, leading to anatase TiO_2 with a narr ize di tion. Further-more, due to rapid and homogene microwave ing, a better crystallinity can be obtained. T high-quali O_2 single-crystals exposed with (0 0 1) fa ets can ynthesized with a high yield [64]. Their results de nstrated also t the F^- rich environment, attributed to th ic liquid, is a key terminant to form (0 0 1) facets expose atase 2 single crystals. When the content of ionic liquids rea rom 0.14 M to 0.54 M, the ratio of surface area of reactive) facets otal surface area increased from 27 to 5 conc d th he more bulky (BF_4^-) groups can prom the p erred g of the (0 0 1) facets.

In third thesis rou e, fluorine species (e.g. HF) are introduc agent to reduce surface energies of anatase Ti pecially (0 0 1) facets, which leads to a large percentage of th ctive (0 0 1) facets exposed in final assemblies or films of titan ith the largest exposure area. Wu et al. proposed possible reactions involved in the Ti–HF interactions under a hydrothermal condition include [65]:

$$Ti + 6HF \rightarrow H_2TiF_6 + 2H_2\uparrow \quad (1)$$

$$H_2TiF_6 + 4H_2O \rightarrow Ti(OH)_4 + 6HF \quad (2)$$

$$Ti(OH)_4 \rightarrow TiO_2\downarrow + 2H_2O \quad (3)$$

Anatase nanocrystals shaped as truncated bipyramids are generally achieved in such a HF-mediated synthesis. Wu et al. investigated that HF acts as a corrosive to attack the Ti plate to release finally Ti(IV)-hydrates into the reactants for titania precipitations; at the same time, the selective absorption of F^- ions on the (0 0 1) facets of anatase crystals achieved the formation of truncated bipyramids [65]. They also observed that the increasing HF concentration not only resulted in more Ti(IV)-hydrates in solutions, but also enhanced retarding effects for the vanish of facets other than (0 0 1) during the crystal growth; therefore, it is not surprising that an increasing HF concentration favored the growth of larger anatase single crystals with the shape of highly truncated bipyramids [65].

Gordon et al. reported non aqueous surfactant-assisted solvothermal synthesis of highly uniform anatase TiO_2 nanocrystals (NCs) with tailorable morphology in the 10–100 nm size regime, prepared through a seeded growth technique [66–68]. Small TiO_2 nanocrystallites (or "seeds") are firstly formed by combining a small quantity of titanium(IV) halide (TiX_4) dissolved in oleic acid (OLAC) with a large molar excess of the co-surfactant (oleylamine (OLAM) or 1-octadecanol (1-ODOL) in solvent 1-octadecene (1-ODE) and quickly heating to 290 °C under nitrogen atmosphere [66]. This method was described to design the percentage of (0 0 1) and (1 0 1) facets through the choice of co-surfactant and titanium precursor and to demonstrate that the choice of both titanium precursor and co-surfactants dramatically influences the morphology of TiO_2 NCs. Gordon et al. suggested, that in the first step of the synthesis, the dissolution of TiX_4 precursors occurs in the presence of OLAC [66]. It is known from the literature that short chain carboxylic acids have been shown to complex with $TiCl_4$ at low temperature in non-aqueous solutions, resulting in the formation of stable mono- and polynuclear chlorotitanium carboxylate complexes and the release of HCl [69]. Authors expect that the coordination of OLAC with titanium centers upon dissolution of titanium(IV) halides (TiX_4) into solutions of OLAC/1-ODE, releasing hydrohalic acids (HX) into the solution. In the case of TiF_4, this translates to the *in situ* release of

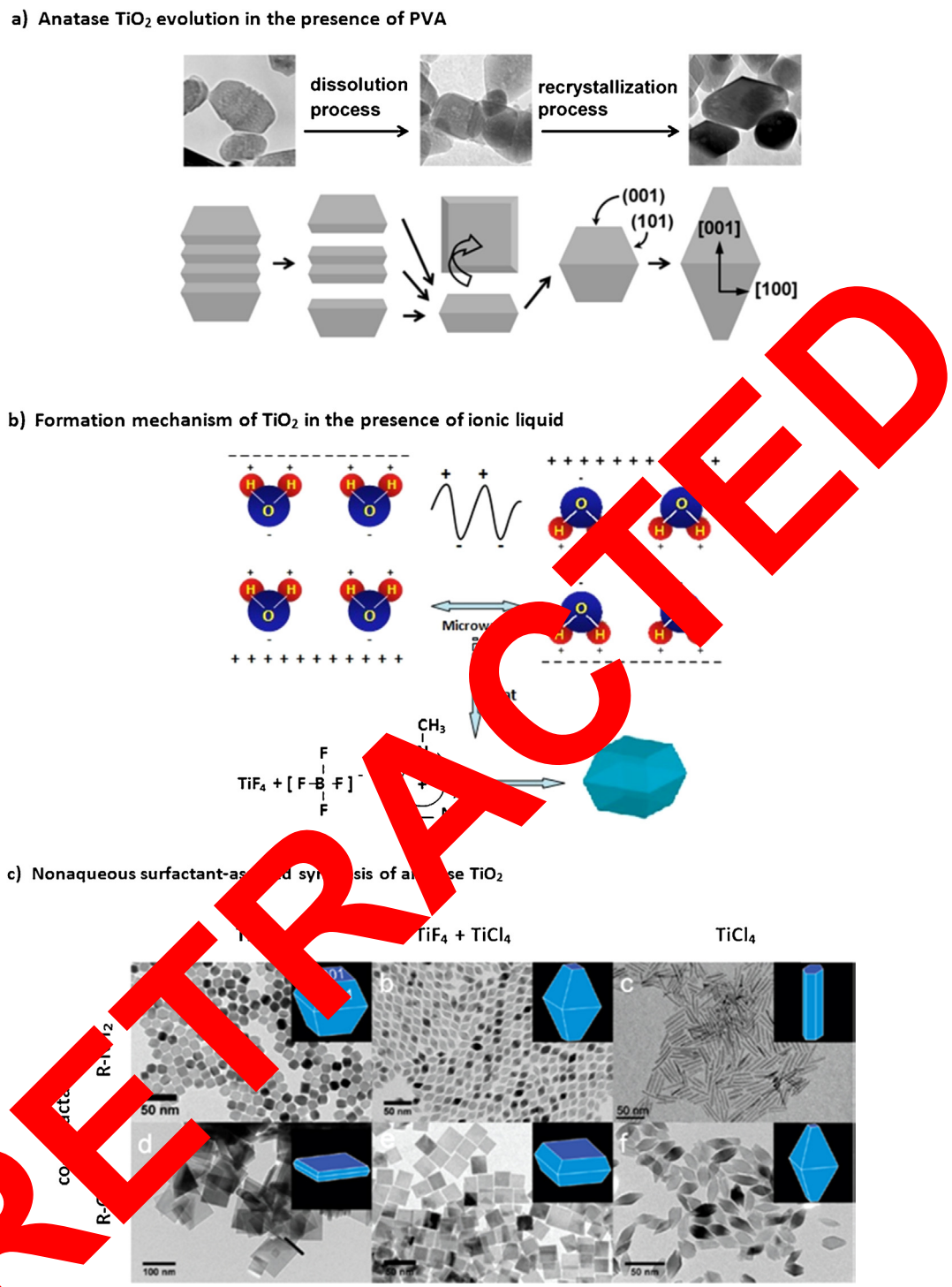

Fig. 3. Schematic route ape evolution of TiO_2 with exposed (0 0 1) facets in the presence of: (a) PVA (adapted from ref. [40]), (b) ionic liquid and microwaves (adapted from ref. [64]), and (c) dif rent co-surfactants and different TiO_2 precursors (TiCl4 and TiF4) (adapted from ref. [66]).

HF, which acts as a shape directing agent, providing the fluoride ions which bind selectively to the {0 0 1} facet of anatase TiO_2 and manipulate the shape of the nanoparticles [66]. They found, that depending on the choice of co-surfactant and titanium(IV) halide (TiX_4) under otherwise identical reaction conditions, the following nanostructures could be obtained (Fig. 3c):

- highly uniform tetragonal bipyramidal anatase (co-surfactant: oleylamine; precursor: TiF_4),
- pure phase brookite nanorods (co-surfactant: oleylamine; precursor: $TiCl_4$),
- anatase nanoplates with a high percentage of {0 0 1} facets (co-surfactant: 1-octadecanol; precursor: TiF_4),
- tetragonal bipyramidal anatase with primarily {1 0 1} facets (co-surfactant: 1-octadecanol; precursor: $TiCl_4$),
- monodisperse anatase tetragonal bipyramidal nanoparticles with small percentage of (0 0 1) facets (co-surfactant: oleylamide; precursor: mixture of $TiCl_4$ and TiF_4),

- nanoplates with large percentage of (0 0 1) facets (co-surfactant: 1-octadecanol; precursor: mixture of $TiCl_4$ and TiF_4) [66].

Even more green route to prepare decahedral-shaped anatase *via* gas phase reaction of $TiCl_4$ with O_2, without adding any fluorine compounds, was developed by Ohtani group [37,60]. They showed, that the decahedral-shaped anatase particles with primary particle size of 70 nm can be prepared by using either a burner or an electric furnace in a gas phase reaction process comprising rapid heating and rapid quenching conditions.

The density, size distribution and surface chemistry of the resulting crystalline nucleus is highly dependent on the reaction environment of the solution. The morphological structure including percentage content of (0 0 1) facets can be modified by changing preparation conditions and it is well established that solvents, impurities and additives in solution can substantially influence the ultimate shape of the crystals. In summary, the solvent effect on the crystal shape is generated *via* the varied solvent–solute interactions along different orientations of a crystal. This is because surface atomic arrangement and thus surface affinity for the solvent to each orientation is different, which can certainly affect the growth rates to the crystal surfaces and hence the final shape of the crystal [61].

3. Oxidation and reduction sites on TiO_2 particles

Ohno et al. reported that oxidation site and reduction site on the rutile particles are on the (0 1 1) face and on the (1 1 0) face, respectively [35]. For anatase particles, they suggested that the (0 0 1) face provides the effective oxidation site, while the (0 1 1) face works as the reduction site [35]. Thus, they expected different energy levels of the conduction and valence bands for different crystal faces of TiO_2 because of the atomic arrangements characteristic of these faces. The difference in the energy levels d... the electrons and holes to different crystal faces ... to separation of electrons and holes. This separation ... probably the key ... the high efficiency of some photocatalytic reactions ... as water oxidation, which require band bending ... TiO... indicated that different energy levels of ... duction ... valence bands, which are determined by the arrangement and kind of constituent atoms, drive the electrons and ... holes to different exposed crystal faces, resulting in a decrease in ... back-reaction rate by predominant progress of ... duction and ... tion on each crystal face.

It has been evidently detected that the photoelectrons selectively migrated toward (1...) facets, while photo-induced holes tended to (0 0 1) facets. ... more •O... radicals would be generated on (0 0 1) fa... more ... cals might be formed on (1 0 1) facets [7... Beside... the contri...on from the enhance dissociative adsorp... medi...by (0 0 1) facets, separation of photoexcited hole/elec... ...oted by these (0 0 1) facets. First, the surface def... (e.g., oxygen vacancy) play an important role in mediating the ...facial electron transfer and thus photocatalytic activity. High-energy (0 0 1) facets are typically characterized by high densities of under-coordinated Ti atoms and very large Ti-O-Ti bond angles, giving rise to abundant oxygen deficiency [71]. Therefore, it is not surprising that with increasing the percentage of (0 0 1) facets (from nanoparticles (ca. 10%) to nanosheets (ca. 70%)), the photocatalytic activity first rapidly increases. However, when the percentage of (0 0 1) facets exposed is higher than 70%, the photocatalytic activity markedly decreases [54]. This is because the lower percentage of (1 0 1) facet is not beneficial for the transfer and separation of photogenerated electrons and holes and their synergistic effect on photoactivity. Therefore, it is not difficult to understand that the relative percentage of the exposed (0 0 1) and (1 0 1) facets is a very important parameter for the effective separation of photogenerated electrons and holes and has a significant influence on the photocatalytic activity [52].

Murakami et al. photodeposited Pt and PbO_2 on anataseTiO_2 to determine the sites on which reduction or oxidation predominantly proceeds [40]. The color of TiO_2 powders after UV irradiation in the presence of H_2PtCl_6 and $Pb(NO_3)_2$ aqueous solution changed to gray and brown, respectively, suggesting that Pt and PbO_2 were deposited on the TiO_2 surface. Pt particles (from the photoreduction of Pt^{4+}) of a few nanometers in size were mainly observed on the (1 0 1) face of decahedral anatase, while PbO_2 (from the photooxidation of Pb^{2+}) particles of ca. 10 nm in size were mainly deposited on the (0 0 1) face of decahedral anatase. These results are in good agreement with results of a previous ...ed by Ohno et al. showing that oxidation and reduc... predom...tly proceed on (0 0 1) and (1 0 1) faces of decah... anatase ..., respectively (Fig. 4b and d) and on the (1 1 1) ... and on t... (1 1 0) face of rutile nanoparticles (Fig. 4... d c) [35].

Decahedral TiO_2 wi... small $d_{(...24)}$ (Fig. ... has a larger surface area of oxidation site... d sm... surface area of reduction sites, while decahedral TiO_2 v... ge $d_{A(00...}$ (Fig. 5b) has a smaller surface area of oxi...on sites ... larger ...face area of reduction sites. Thus, a trad... relation exis... een surface area of oxidation and redu... s [40].

However, the ...hesized shape-controlled anatase TiO_2 prepar... Murakami ... had a primary particle size of ca. 25 nm, ... is thought to be ...sufficient for separation of redox sites. ...us, an increase in the particle size of a shape-controlled nanocrystal will possib...nhance photocatalytic activity as a result of more ...tive sepa...on of redox sites (see Fig. 5) [38].

...ak... et al. have also reported that shape-controlled rutile rod al... photocatalytic activity depended on their surface structure, which could be controlled by using shape-control reagents ...mical etching [72]. These rutile rods predominantly have (1 1 0) and (1 1 1) exposed crystal faces, which were respectively attributed to reduction and oxidation sites (see Fig. 6).The rutile rods had aspect ratios of over five due to preferential growth along the (0 0 1) direction, indicating that they had a large (1 1 0) surface area and a small (1 1 1) surface area. A surface structure with a larger surface area of reduction sites than oxidation sites may be desirable for pristine rutile TiO_2 because the bottleneck reaction for conventional organic decomposition under aerated conditions is presumably oxygen reduction rather than oxidation because of the conduction and valence band potentials of rutile TiO_2. This tendency is possibly more pronounced for rutile than anatase since the conduction band of rutile is less negative than that of anatase. One plausible reason for relatively high photocatalytic activity of the rutile may be because multielectron reduction of oxygen occurs as a result of separation of redox sites which was induced by specific exposed crystal faces. Therefore, it should be possible to further enhance photocatalytic reactions by optimizing the aspect ratio of the rods. The results indicate that the oxidation site and the reduction site on the rutile particles are on the (0 1 1) face and on the (1 1 0) face, respectively.

It was well documented that surface fluorination can enhance the photocatalytic activity of TiO_2 due to the formation of free hydroxyl radicals, which are more mobile than those generated on pure TiO_2 under UV irradiation [50,73]. Zheng et al. reported on the rapid synthesis of anatase TiO_2 nanocrystals with a continuously tunable percentage of reactive (0 0 1) facets *via* a microwave enhanced thermal [74]. To study the effect of surface fluoride ions on the photoactivity of TiO_2 nanosheets with exposed (0 0 1) facets, the fluorinated surface of TiO_2 nanosheets was cleaned by washing with NaOH diluted solution. It has been reported that the adsorbed fluoride ions on the surface of TiO_2 can be easily removed by alkaline washing in a NaOH solution without altering the crystal structure and morphology [54]. This is due to the fact that

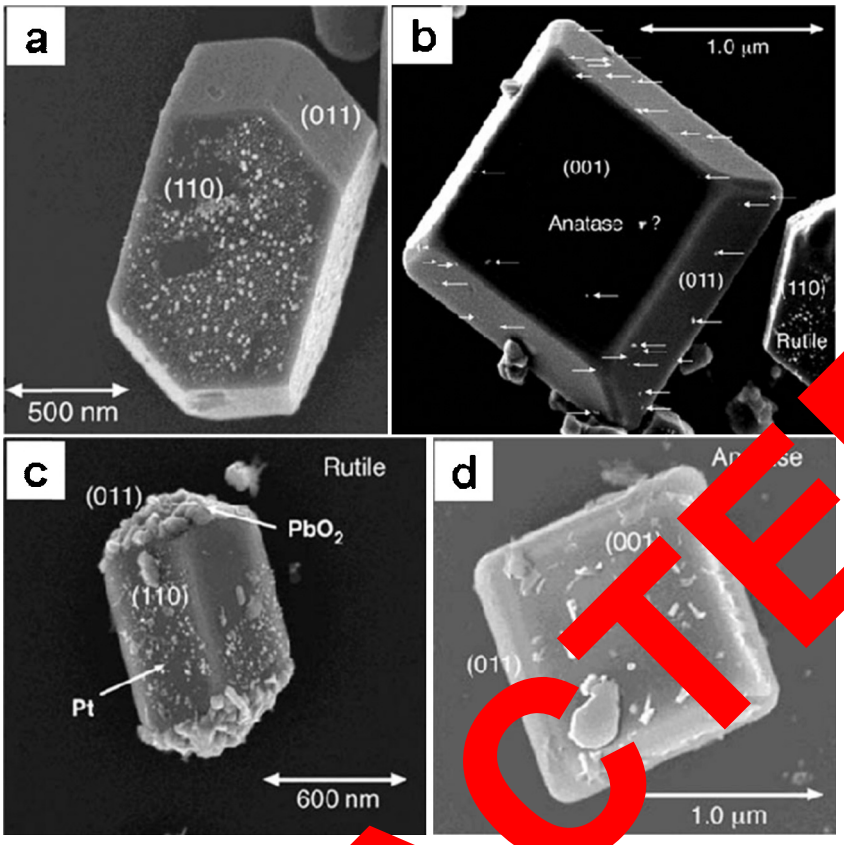

Fig. 4. SEM images of a rutile particle (a) and an anatase particle (b) loaded with Pt nanoparticles deposited via UV-irradiation in a solution of 1.0 mM H_2PtCl_6. SEM images of a rutile particle (c) and an anatase particle (d) modified by PbO_2 deposits via UV-irradiation of the Pt-TiO_2 powder in a solution of 0.1 M $Pb(NO_3)_2$. These results showing that oxidation and reduction predominantly proceed on (0 0 1) and (1 0 1) faces of bipyramidal anatase TiO_2, respectively (b and d) and on the (0 1 1) face and on the (1 1 0) face of rutile nanoparticles (a and c). Reprinted from ref. [35].

F^- on the surface of TiO_2 nanosheets is remove[illegible] a sim[illegible] ligand exchange reaction between OH^- in the NaO[illegible] TiO_2. Zheng et al. observed that with inc[illegible] exposed (0 0 1) facets, the positive effe[illegible] on the photocatalytic activity of high-energy Ti[illegible] ocrystals be[illegible] more obvious [74]. The positive effect o[illegible] fection was attributed to the formation of free hydrox[illegible] radicals [5[illegible] while the negative effect of fluoride effection w[illegible] scribed to the i[illegible] ance adsorption of the dye (used in photocatalytic process) due to the competitive adsorption between dye and fluoride ions [74].

Though the detailed mechanism of the face-selective electron and hole separation is still in its infant stage, the selective photocatalysis on anatase TiO_2 crystals with specific exposed crystal faces opens a pathway to a deeper understanding of various photocatalysis processes. The proposed reason for different facets as oxidation and reduction sites is that surface energy levels (namely, surface electronic structures) of the conduction bands and valence bands of facets are different so that photoexcited electrons and

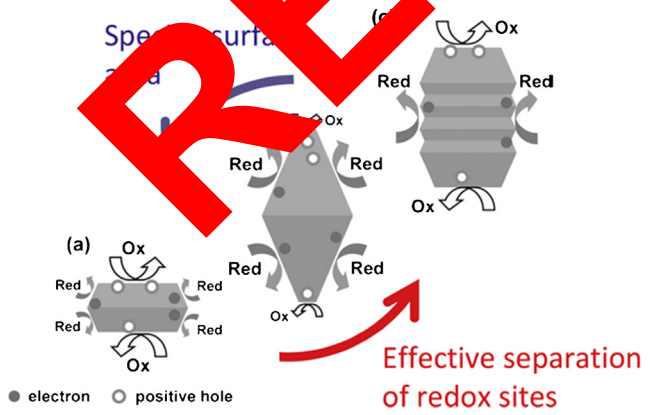

Fig. 5. Schematic images of spatial separation of redox sites on anatase TiO_2 particle with specific exposed crystal face based on Murakami et al. [38,40]: (a) decahedral particle with a larger surface area of oxidation sites and smaller surface area of reduction sites; (b) decahedral particle with a smaller surface area of oxidation sites and larger surface area of reduction sites; and (c) stacked-structured particle with larger surface area of both oxidation and reduction sites.

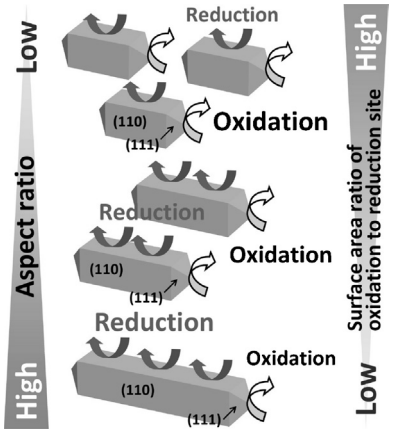

Fig. 6. Dependence of aspect ratio of shape-controlled rutile rods on surface area ratio of oxidation to reduction sites, which possibly affects the photocatalytic properties. Reprinted from ref. [72].

holes can be driven to different facets, leading to the separation of electrons and holes.

4. Preparation, characterization and photocatalytic activity of decahedral anatase titania particles

The surface stability and photoreactivity of inorganic single crystals have long been thought to be dominated by their surface chemistry, whose effect on the equilibrium morphology is critical for the synthesis of single crystals with high photoreactivity. For anatase TiO_2, both theoretical and experimental studies found that the minority (0 0 1) facets in the equilibrium state are especially reactive.

An important breakthrough in preparation of anatase TiO_2 sheets with exposed (0 0 1) facets was achieved by Yang et al. [71]. They reported the synthesis of anataseTiO_2 single crystals with 47% of exposed (0 0 1) facets using hydrofluoric acid as a shape controlling agent. To further explore the effects of various adsorbate atoms, Yang et al. carried out a systematic investigation of 12 non-metallic atoms X (where X can represent H, B, C, N, O, F, Si, P, S, Cl, Br or I) based on first-principle calculations. Fig. 7a–d illustrates the models of clean and X-terminated (0 0 1) and (1 0 1) surfaces and the calculated surface energy values for different adsorbates are shown in Fig. 7e. Yang et al. observed that: among the 12 X-terminated surfaces and the clean surfaces, termination with F atoms not only yields the lowest value of γ for both the (0 0 1) and (1 0 1) surfaces, but also results in (0 0 1) surfaces that are more stable than (1 0 1) surfaces. These results indicate that it might be possible to achieve anataseTiO_2 single crystals with a high percentage of anatase (0 0 1) facets if their surfaces are surrounded by F atoms [71].

To verify these theoretical predictions, Yang et al. obtained [illegible]cated anatase bipyramids. They used titanium tetrafluoride (TiF_4) aqueous solution and hydrofluoric acid as the anatase single c[illegible]tals' precursor and crystallographic controlling [illegible]spectiv[illegible] to prepare anatase TiO_2 single crystals [71]. O[illegible]e basi[illegible] the sy[illegible]metries of anatase TiO_2, the two flat, squar[illegible]faces [illegible]he (0 0 1) facets and the eight isosceles trapezoid[illegible] sur[illegible] (1 0 1) facets of the anatase TiO_2 single crystals. [illegible] yield o[illegible]tase TiO_2 single crystals is around 90%, even th[illegible] some aggl[illegible]ates and/or irregular particles were occasi[illegible]y [illegible]rved [71].

Moreover, Yang et al. observed th[illegible] crystal facet control was observed in the abse[illegible] of hydrofluo[illegible]id, and only hollow spherical polycrystalli[illegible]natase particles w[illegible] formed. Hydrofluoric acid is believed [illegible] have [illegible] roles here: to retard hydrolysis of the titanium precu[illegible]a[illegible]o reduc[illegible] surface energy to promote the isotropic growth alo[illegible]e (0 1 0) and (1 0 0) axes.

To inves[illegible]e pho[illegible]ctivity of (0 0 1) facets experimentally, TiO[illegible]ingle [illegible]stals wi[illegible]ominant (0 0 1) facets should be obtain[illegible]uce th[illegible]fluence of contributions of (1 0 1) facets.

To so[illegible]al issue, Yang et al. reported a new solvotherm[illegible]ethod using 2-propanolas a synergistic capping agent and rea[illegible] medium together with HF to synthesize high-quality anatase TiO_2 single-crystal nanosheets (SCNSs) with 64% of the (0 0 1) facets (experimental conditions see in Table 1) [75]. Diffraction pattern indicated that the sample is in form of a pure anatase. From the symmetries of the well-faceted crystal structure of the SCNSs, the two flat square surfaces were identified as (0 0 1) facets while the other eight isosceles trapezoidal surfaces were (1 0 1) facets. The average size of the anatase TiO_2SCNSs was 1.09 μm with a thickness of 260 nm, and the percentage of (0 0 1) facets is 64% on average [75]. Chemical compositions of anatase TiO_2 SCNSs were analyzed with X-ray photoelectron spectroscopy. The XPS spectrum of F 1s core electrons shows that the binding energy (BE) is 684.5 eV, which is a typical value for the fluorinated TiO_2 system such as ≡Ti-F species on the TiO_2 crystal surface. The C 1s spectrum shows a component at a BE of 286.4 eV, which may result from surface oxidation of the aliphatic chains and adsorbed isopropoxide species. The C 1s peak at 284.7 eV can be assigned as aliphatic hydrocarbon, and the smaller peak at BE of 288.7 eV is due to the presence of carboxylate impurities [75].

The efficiency for heterogeneous photocatalytic reaction of anatase TiO_2 SCNSs synthesized with a reaction time of 22 h was monitored by measuring the formation of active hydroxyl radicals (•OH) upon irradiation. Significant fluorescence spectra associated with 2-hydroxyterephthalic acid (TAOH) were generated upon irradiation within 220–770 nm. The linear relationship between fluorescence intensity and irradiation time confirms the stability of anatase TiO_2 SCNSs. Yang et al. exami[illegible]ability of forming •OH per unit surface area of anata[illegible]O_2 SCNS[illegible]P25. Concentration of •OH generated from SCNS[illegible]h clean sur[illegible]s is more than 5 times higher than that of D[illegible]ussa[illegible]TiO_2.The[illegible]sults indicated enhanced photoreactivity[illegible]the anata[illegible]iO_2 [illegible]SNSs with a large percentage of (0 0 1) f[illegible]s, whi[illegible] can b[illegible]buted to the high density of unsaturat[illegible]fold [illegible]s well as their unique electronic structure [75].

Based on [illegible]g et al.[illegible]dy, A[illegible]o et al. obtained single-crystalline [illegible]se particles[illegible]a gas-phase reaction with relatively[illegible]gh [illegible]d of decahe[illegible]l particles and recognized that photocatalytic effi[illegible]cy depends on surface area, if the reaction rate[illegible]pressed by [illegible]order kinetics with respect to the amount [illegible]rface-adsorbed rea[illegible]ants and the amount increases with an [illegible]crease in surface area [60]. TiO_2 crystallites were fabricated from [illegible]anium(IV) [illegible]oride by a gas-phase reaction process with rapid [illegible]ing (see T[illegible]e 1). The TiO_2 particles generated by thermal oxida[illegible]of Ti[illegible] were collected at the downstream by a filter cup made [illegible]lass fibers. Uniform and rapid heating at a high temperature would enable homogeneous nucleation and subsequent [illegible]r to well faceted crystals with few defects. The low concentration of $TiCl_4$ and the narrow heating zone would prevent formation of large particles and polycrystalline aggregates with grain boundaries [60].

The powder X-ray diffraction pattern indicated that there are anatase crystallites and a small amount of contamination of rutile crystallites. Ahonen et al. also reported that gas-phase crystallization of titanium(IV) tetra-2-propoxide at 1200 °C involves formation of minor rutile crystallites in addition to single-crystalline anatase particles with (1 0 1) and (0 0 1) facets [76]. Photocatalytic activity of the samples was evaluated by two photocatalytic reactions in aqueous solutions: (a) hydrogen evolution from an aqueous methanol (MeOH) solution containing precursors for *in situ* photodeposition of Pt, and (b) oxidative decomposition of acetic acid (AcOH) and MeOH in air. Using H_2PtCl_6 as a Pt precursor, it was observed that the amount of H_2 increased linearly with irradiation time and the rate of H_2 evolution was higher in the presence of decahedral single-crystalline particles than that by P25. When $(Pt(NH_3)_4)Cl_2$) was used as a Pt precursor instead of H_2PtCl_6, the rate of H_2 evolution was decreased and an induction period of ca. 30 min was observed for both types of TiO_2 [76]. Ohno et al. reported that Pt particles were preferably deposited on micrometer-sized decahedral anatase particles in the order of (1 0 1) > (0 0 1) ≫ (1 1 2) in photocatalytic reduction of H_2PtCl_6 using 2-propanol as an electron donor [35,55]. Amano et al. also observed that Pt particles were deposited both on (1 0 1) and (0 0 1) facets. For oxidative decomposition of acetic acid in an aerated aqueous suspension in the presence of single-crystalline anatase particles, the amount of CO_2 linearly increased with irradiation time and the decahedral single-crystalline particles exhibited a rate of CO_2 liberation as high as that of P25. In the case of methanol decomposition, the amount of CO_2 liberation over single-crystalline anatase particles was much larger than that of P25. The difference between the photocatalytic activity of DSC particles and

Table 1
Summary of SEM/TEM images, particle size, synthesis conditions and photocatalytic activity of anatase TiO_2 crystals with exposed crystal facets.

SEM/TEM image	Particle/crystalsize	TiO_2 precursor	Synthesis parameters	Model compound and its initial concentration	Experimental con[illegible]	Photocatalytic acitivity	Ref
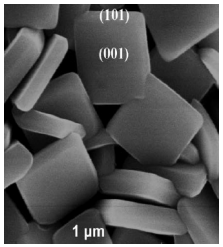	Size: 1.09 μm, Thickness:260 nm	TiF_4	Precursor: 14.5 ml (2.76 mM) TiF_4, Morphology controlling agent: 0.5 ml HF, 10% w/w Procedure: hydrothermal process, 180 °C, 5.5–44 h Calcination:600 °C, 1.5 h	Terephthalicacid (3 mM)	T[illegible]otocatal[illegible]as susp[illegible]l in 40 [illegible] aqueous solutio[illegible]ai[illegible]g 0.01 M NaOH and [illegible]Mterephthalic acid [illegible]radiation source: 300 W Xe [illegible] (λ = 320 nm)	Fluorescencesignal intensity of the 2-hydroxy terephthalic acid was about: 45 a.u. (5 times more active than P25)	[75]
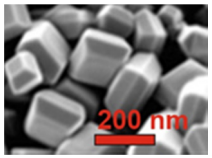	Size: 50–250 nm	$TiCl_4$	Precursor: $TiCl_4$ vapor generated by bubblingargon (200 ml min^{-1}) into $TiCl_4$ solution at358 K m[illegible] O_2(1200 ml min^{-1}) Procedure: CVD, 15[illegible]	[illegible]) [illegible]drogenevol[illegible]n [illegible] Me[illegible]on under argon (b) [illegible]lative d[illegible]mposition of AcOH and MeOH in air	50 mg of TiO_2 and 2 wt% of H_2PtCl_6 (for in situphotodeposition of Pt) Irradiation source:400 W high-pressure mercury lamp	H_2 evolution: showing a higher rate than P25 TiO_2, in particular in the presence of $[Pt(NH_3)_4]Cl_2$ under 400 W high-pressure mercury lamp; Photodecomposition capability: as high as that of P25 for decomposing acetic acid, much higher than P25 for decomposing methanol.	[60]
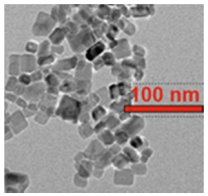	Size: 21.5 nm, Thickness: 12.7 nm	$Ti(OC_4H_9)_4$	Precurs[illegible]g $Ti(OC_4H_9)_4$, Morpholog[illegible]ntrolling agent: 2 ml of HF [illegible]rocedure: hydrothermal [illegible]ess, 200 °C for 24 h. D[illegible]ng: 80 °C, 10 h	Coumarin (0.5 mmol dm^{-3})	Irradiation source: UV irradiation (λ = 332 nm)	The photocatalytic activity of high-energy anatase TiO_2 nanocrystals increases with increasing the amount of HF solution due to the exposed high-energy {0 0 1} facets and surface fluorination.	[53]
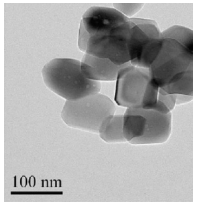	–	$Ti(OC_4$[illegible]	Precursor: 50 g $Ti(OC_4H_9)_4$, Morphology controlling agent: 8.0 ml HF, 40 wt% Procedure: hydrothermal process, 200 °C, 24 h Drying: 80 °C, 10 h Calcination: 300–1250 °C	Acetone (300 ppm)	Dishes coated with TiO_2 powders (0.3 g of photocatalyst) were placed in photoreacotr (15 dm^3) Irradiation source: 15 W, 365 nm UV lamp	With increasing the calcination temperature to 600 °C, the photocatalytic activity of TiO_2 decreases. The photocatalytic activity of TiO_2 begins to increase after calcined at 700 °C (4.79×10^{-3} min^{-1} for T700)	[51]

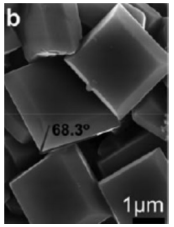	Size: 1.1–3.1 μm thickness: 1.6–1.8 μm	$TiOSO_4xH_2O$	Precursor: 64, 32, 32 mg $TiOSO_4xH_2O$ Morphology controlling agent: 120, 80, 40 mM HF Procedure: hydrothermal process, 180 °C, 2–12 h. Drying: 80 °C, 12 h Pt loading: impregnation method, Pt precursor: $H_2PtCl_6{\cdot}6\,H_2O$, (1 m[illegible] Pt)	1. tereph[illegible]c ac[illegible] (3 mM) meth[illegible]ol (10 vol)%	1. 5 mg of p[illegible]tocatalyst were [illegible]uspended in 80 ml aqueous [illegible]ution containing 0.01 M [illegible] and 3 mM terephthalic acid, Irradiation source: 300 W Xe lamp (λ = 320 nm) 2. 100 mg of the TiO_2 (deposited with 1 wt% $H_2PtCl_6{\cdot}6H_2O$) powder were dispersed in 300 ml aqueous solution containing methanol	Fluorescence signal intensity of the 2-hydroxy terephthalic acid was about: 25-65a.u. H_2 evolution: about 15–40 μmol h^{-1}	[39]
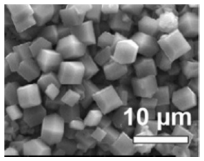	Size: 2.4–13.6 μm	Titanium plates (2 cm × 2 cm × 0.2 cm, obtained from sheet of commercial pure titanium TA2 (w[illegible] the purity of [illegible])	Precu[illegible]ium pla[illegible] M[illegible]ology [illegible]trolling [illegible]: [illegible]–0.80% H[illegible]5 mass% [illegible]edure[illegible]al p[illegible] Dry[illegible]°C	Rhodamine B (0.005 mM)	Irradiation source: 20 W UV lamp (λ = 365 nm) Illumination time: 120 min	The reaction rate constant: 5.5, 4.8 and 6.6 × 10^{-3} min^{-1} respectively, for the three immobilized anatase layers derived by the hydrothermal reactions for 3, 12 and 24 h.	[65]
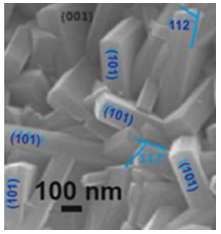	Particle size: 600 nm Thickness: 130 nm	[illegible]$(OC_4H_9)_4$ [illegible]$(NH_4)_2$[illegible]	Precursor: 1 ml $Ti(OC_4H_9)_4$, 0.25 g $(NH_4)_2TiF_6$ Procedure: hydrothermal process, at 150–180 °C for 24 h Drying: 80 °C, 12 h Calcination:600 °C for 2 h	Terephthalic acid (5×10^{-4} mol/dm^3)	300 W high pressure xenon lamp UV light (λ = 365 nm)	101/001–1 possessed about 8 and 4 times higher photocatalytic oxidation and reduction activity respectively, in comparison to 010/001–1	[79]

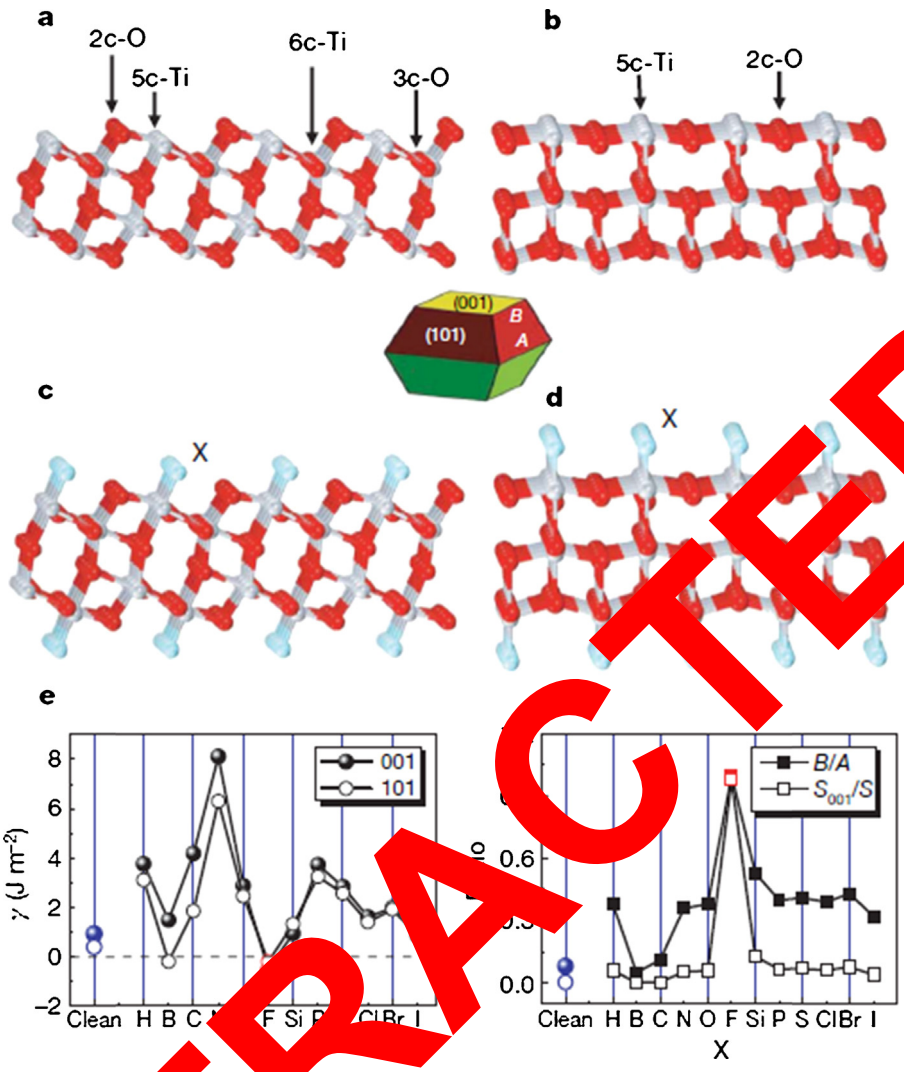

Fig. 7. Slab models and calculated surface ener… of anatase Ti… 01) and (1 0 1) surfaces. The optimised ratios of B/A and percentage of {0 0 1} facets (S001/S), where S and S001 are respectively the total surface a… that contribute… he {0 0 1} facets, are also shown. (a, b) Unrelaxed, clean (0 0 1) and (1 0 1) surfaces. Ti and O atoms are represented by grey and red spheres… six… i, fivefold Ti, t… efold O and twofold O labelled as 6c-Ti, 5c-Ti, 3c-O and 2c-O, respectively. (c, d) Unrelaxed (0 0 1) and (1 0 1) surfaces surrounded by adsorbate X atoms. (e) Calculated energies of the (0 0 1) and (1 0 1) surfaces surrounded by X atoms. (f) Plots of the optimized value of B/A and percentage of {0 0 1} facets for … se single crysta… h various adsorbate atoms X. In e and f, clean-surface results (denoted by blue spheres and circles) are used for reference. As indicated in the ins… gram, two independ… arameters A and B denote lengths of the side of the bipyramid and the side of the square {0 0 1} 'truncation' facets, respectively. The ratio… ghly re… e {0 0 1} facets to total surface area may therefore be described by the value of S001/S or B/A (where $0 \leq B/A \leq 1$). Reprinted from ref. [71].

that of P25 se… ificant… m… anol decomposition rather than acetic … deco… osition. … no et al. noted that white P25 particles … ed blu… mediately after commencement of photoirradiation d… … methanol oxidation, which was not observed for … edral single-crystalline particles. The blue color is attributable to … formation of reduced species of Ti^{4+} (Ti^{3+}) and indicates that e… rons are accumulated in P25 particles even in the presence of molecular oxygen as an electron acceptor. Efficient electron transfer to oxygen at the surface of DSC particles may account for their better or comparable photocatalytic activity [76].

Murakami et al. [40] and Ohno et al. [35] showed that different surface energy levels of the conduction and valence bands are expected for different crystal facets of TiO_2 because of the atomic arrangements characteristic of these facets. The difference in the energy levels drives the electrons and holes to different crystal faces, leading to separation of electrons and holes, which is very important to the enhancement of the photocatalytic activity. Therefore, it is likely to optimize the photocatalytic activity of anatase TiO_2 by tailoring the exposed high-energy facets.

Wang et al. obtained anatase TiO_2 nanocrystals with exposed high-energy (0 0 1) facets using HF as morphology-controlling agent and investigated the relationship between photocatalytic activity and the percentage of exposed (0 0 1) facets of high-energy anatase TiO_2 nanocrystals (see Table 1) [53]. Physical properties related to the volume of HF added into reaction environment during synthesis and resulted percentage of (0 0 1) facets are shown in Table 2. Based on XRD analysis they observed that broad peak at $2\theta = 25.3^\circ$, corresponding to the (1 0 1) plane diffraction of anataseTiO_2 [53]. With increasing amount of HF to 2 and 4 ml, the peak intensities of anatase increase, indicating an enhancement of crystallization. The presence of fluoride ions at low pH, accelerates TiO_2 crystallization and growth due to rapid *in situ* dissolution–recrystallization processes, which reduces the numbers of defects and impurities in the TiO_2 lattice. However, with further increase in the amount of HF from 8 to 16 ml, the relative crystallinity of anatase TiO_2 decreases, due to the strong affinity of fluoride to titanium, inhibiting the extensive Ti–O–Ti bridging and crystal growth [53].

Table 2
Physical properties of the photocatalysts with exposed (0 0 1) facets obtained by Wang et al. using hydrothermal synthesis. The resulted sample was denoted as HFx, where *x* represents the volumes of HF added into the mixed solution. *Reprinted from ref.* [53].

Photocatalyst	Materials			Characterization results			
	$Ti(OC_4H_9)_4$ (g)	HF (ml)	H_2O (ml)	Percentage of {0 0 1} facets	S_{BET} (m^2/g)	Pore volume (cm^3/g)	Average pore size (nm)
HF0	50	0	8	6	138	0.31	8.8
HF2		2	6	41	82	0.26	10.0
HF4		4	4	63	74	0.23	11.9
HF8		8	0	88	63	0.43	24.1
HF12		12	0	93	45	0.25	19.2
HF16		16	0	96	36	0.14	15.0
HF20		20	0	-	9.3	0.05	14.5

Wang et al. observed also relationship between the average crystalline sizes of the photocatalysts along (0 0 1) and (1 0 0) direction and the amount of HF solution used during the synthesis. It can be seen that the crystalline sizes along (1 0 0) direction steadily increase with increasing the amount of HF, but the crystalline sizes along (0 0 1) direction increase first and then decrease, which further confirms the preferential growth of high-energy anatase TiO_2 nanocrystals along *a*-axis in the presence of the HF (see Fig. 8). It can be seen that the presence of fluoride facilitates the exposure of high-energy (0 0 1) facets of anatase TiO_2, which enhances the growth of anatase TiO_2 nanocrystals along the *a*-axis while restricts the growth along the *c*-axis [53]. The XPS analysis showed that peak located at 684 eV and attributed to the presence of F 1s is found only in samples prepared by using HF during synthesis. The F 1s binding energy peak originates from surface fluoride (≡Ti–F) formed by ligand exchange between F^- and surface hydroxyl groups [53]. The photocatalytic activity of obtained samples was evaluated by a photoluminescence technique using coumarin as a probe m They found, that the activity of the high-energy anatase nan tals is positively related to the percentage of exposed (0 0 1) When the amount of HF is more than 12 ml, the photocata activity of anatase TiO_2 nanosheets is high tha P25. H photocatalytic activity of the high-energy ana TiO_2 ocryst is ascribed to the synergetic effect of expo high r ive (0 0 1 facets and surface fluorination. On the othe gh concentrated HF (20 ml) results in f ormat f cubic $TiOF_2$, which shows very poor photocata activity [5

The thermal stability and of calcina temperature on microstructures and photoca ic activity of anatase TiO_2 nanosheets with dominan 0 1) fa fabricated by hydrothermal treatment of tetra ltitanate in drofluoric acid solution, were investigated b Lv e [51]. SEM age shown in Fig. 9a, confirmed that th atase sa calci at 200 °C consists of well-defined sh shape struct ving a rectangular outline with a side l of a t 100 nm. e growth of anatase TiO_2 nanocrystal and shape e ution (from nanosheets through nanop cles irr r par s), due to the sintering of the sample be observ amples calcined at 800, 1100 and 1250 n both SEM d XRD analysis [51].

They found th crystalline size of the photocatalyst along (0 0 1) direction inc s much faster than that of (1 0 0) direct with enhancement calcination temperature, reflecting that atase TiO_2 nanosheets have preferential growth along the c-axis ring calcin n treatment (Fig. 9). Moreover, it was observed the perce ge of (0 0 1) facets decreases from about 89 to 64% w alcin ons temperature increases from 200 to 800 °C [51]. The p atalytic activity of the TiO_2 samples calcined at different temperature was evaluated by the photocatalytic degradation one in air. It could be clearly observed that sample calcined at 200° shown better activity that P25 (see details Fig. 9B and C). It was also reported that rise of calcination temperature to 600 °C resulted in the photocatalytic activity drop. Temperature enhancement up to 700 °C leaded to activity increase, which is ascribed to the enhanced crystallization. However, with further increase in the calcination temperature, the photocatalytic activity of TiO_2 steadily decreases due to the decrease of BET surface areas and the percentage of the exposed high-energy (0 0 1) facets. Lv et al. found that even after calcination at 1100 °C, the photoactivity of obtained sample still keeps about 60% that of P25. When calcined temperature is higher than 1200 °C, the photocatalytic activity of TiO_2 powders sharply decreases due to the severe sintering of the samples and the formation of rutile phase [51].

Pan et al. synthesized a set of anatase crystals with different percentages of (0 0 1), (1 0 1), and (0 1 0) facets by controlling the synthesis parameters (see Table 1) [39]. The truncated bipyramids (shown in Fig. 10b and c) are enclosed by eight isosceles trapezoidal (1 0 1) and two square (0 0 1) facets. Fig. 10d shows that an additional quartet column is generated at the center of a particle, so that the truncated bipyramid is separated into two parts located at the ends of the column. The shape of these particles is consistent with the predicted morphology enclosed by (0 0 1), (1 0 1), and (0 1 0) facets of anatase [39]. The percentage of different facets of anatase particles obtained by Pan et al. is given in Table 3. The photooxidation and photoreduction activities of the synthesized anatase samples were estimated by evaluating the amount of OH radicals and the rate of hydrogen evolution from the photoreduction reaction. All three samples (T001-F, T101-F, and T010-F) with fluorine-terminated surfaces show very similar abilities for generating OH radicals and their hydrogen-evolution rates are also nearly identical. After removing the surface fluorine atoms, the corresponding fluorine-free samples, showed apparently improved photooxidation and photoreduction capabilities.

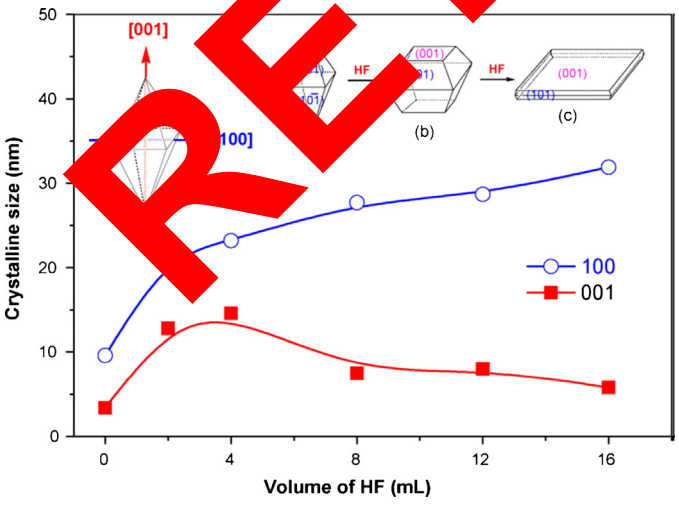

Fig. 8. Dependence of average crystalline sizes of the photocatalysts along (0 0 1) and (1 0 0) direction on the amount of HF solution, indicating that the photocatalyst has the preferential growth along a-axis, whilst the growth along *c*-axis is restrained (inset is the corresponding shape simulation: octahedral bipyramid (a), truncated octahedral bipyramid (b) and nanosheet (c). Reprinted from ref. [53].

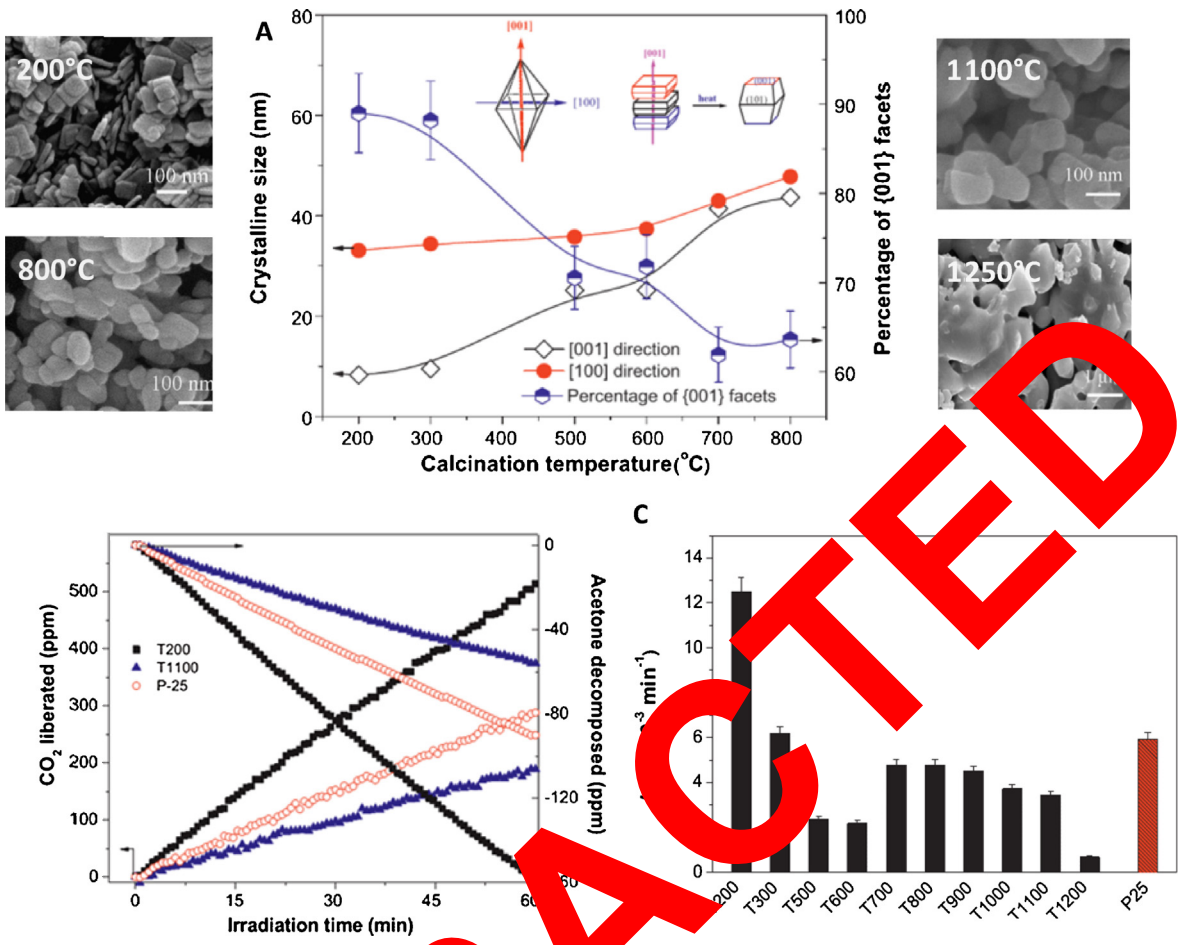

Fig. 9. The effect of calcination temperature on the microstru… …otoactiv… …f anatase TiO_2 nanosheets. with dominant {0 0 1} facets: (A) dependence of average crystalline sizes of the photocatalysts along [0 0 1] and [1… …irectio… …calcinat… …emperatures, together with the percentages of {0 0 1} facets calculated according to geometric shape of Wulff construction, indicating th… …photoc… …yst has the… …eferential growth along *c*-axis ([0 0 1] direction) (inset is the corresponding shape simulation); (B) the dependence of the degraded acetone … …lea… …irradiation time for samples calcined at 200 and 1100 °C and P25 as reference sample, and (C) the photocatalytic activity of the samples ca… …d fro… …1200 °C (p… …todegradation of acetone in air). SEM images of samples calcinated at (a) 200 °C, (b) 800 °C, (c) 1100 °C, and (d) 1250 °C. Reprinted from ref…

Pan et al. concluded that clean (0 0 1), (… …) and (0 1 0) facets follow the photoreactivity o… …r of (0 0 1) < (… …) < (0 1 0). Results obtained by Pan et al. i… …cated that the su… …ce fluorine termination and the per… …ages o… …fferent crystal facets are two determining factors in … …ro… …g the p… …otoreactivity of anatase [39].

Based on … …mic s… …tu… …model of (1 0 1), (0 0 1), and (0 1 0) … …ets, … …y tried … …explain what is the underlying fa… …that … …verses the predicted photoreactivity order of (1… …s, and why do (0 1 0) facets give the highest photo… …vity (Fig. 10). With 100% unsaturated Ti_{5c} atoms at the surface, (0… …facets are theoretically considered more reactive than (1 0 1) wit… …% Ti_{5c} atoms and 50% Ti_{6c} atoms in heterogeneous reactions. As revealed from photocatalytic tests, (0 0 1) has lower photoreactivity than (1 0 1), contrary to the prediction, while (0 1 0), which also has 100% Ti_{5c} atoms exposed, gives the highest photoreactivity among the three facets. UV-Vis absorption spectra (Fig. 10f) showed that the absorption edge of T001 has a red shift of about 6 nm with respect to those of T101 and T010. Results obtained by Liu et al. [77] confirmed that the (0 0 1) facet has a smaller band gap than the (1 0 1) facet due to different atomic configurations. Because absorption edge of T101 and T010 with dominant (1 0 1) and (0 1 0) facets nearly overlap, that is, (0 1 0) and (1 0 1) facets have very close band gaps. X-ray photoelectron valence-band (VB) spectra (Fig. 10g) reveal that VB maxima of all three TiO_2 crystals are at 1.93 eV, that is, the conduction-band (CB) minimum of T101 and T010 is raised in contrast to T001. Fig. 10h showed the resolved band structures of different crystals. The absence of reduction states and upward shift of VB maxima in measured VB spectra are attributed to the negligible amount of oxygen vacancies in TiO_2 samples. Pan et al. observed that (0 1 0) facets have both a favorable surface atomic structure and a surface electronic structure, so that the more strongly reducing electrons in the CB can be transferred *via* the surface Ti_{5c} atoms as active reaction sites. The efficient consumption of excited electrons in the photoreduction reactions can simultaneously promote the involvement of holes in photooxidation reactions. Such a cooperative mechanism existing on (0 1 0) facets is responsible for its having the highest photoreactivity [39].

Wu et al. reported the hydrothermal synthesis of (0 0 1)-exposed anatase single crystals through reactions of Ti plates in aqueous HF

Table 3
Average percentages of {0 0 1}, {1 0 1}, and {0 1 0} facets in T001-F, T101-F, and T010-F, calculated from the surface area of each facet from SEM images [39].

Sample	{0 0 1}	{1 0 1}	{0 1 0}
T001-F	49%	60%	0%
T101-F	24%	76%	0%
T010-F	14%	33%	53%

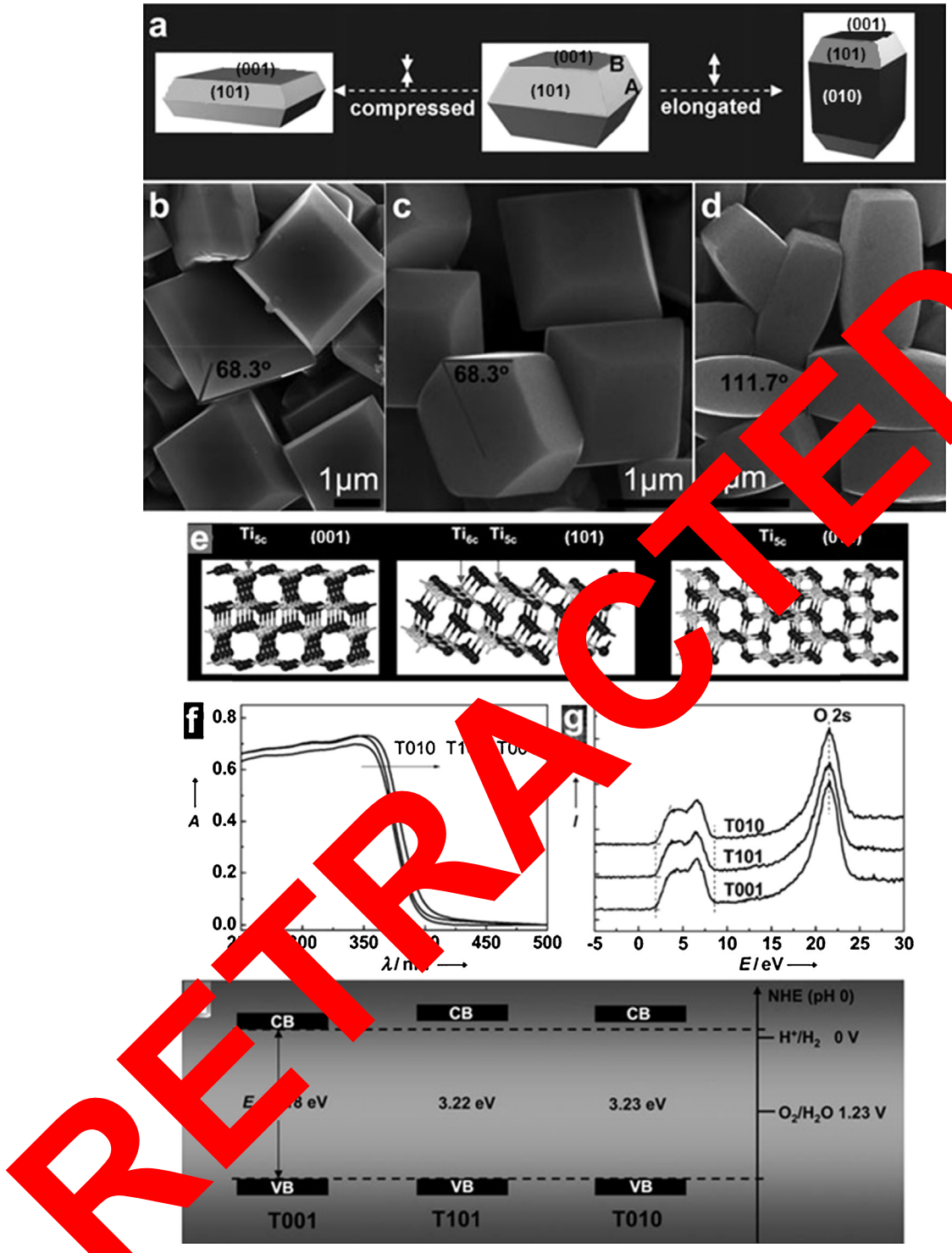

Fig. 10. Morphology and atomic structure of anatase TiO_2 crystals obtained via hydrothermal route: (a) schematic of anatase TiO_2 with different percentages of {1 0 1}, {0 0 1}, and {0 1 0} facets; (b–d) SEM images of anatase crystals synthesized with different aqueous solutions of HF (120, 80, and 40 mM) containing different amounts of TiOSO4 precursor (64, 32, and 32 mg) at 180oC for different times (12, 12, and 2 h). The samples shown in (b–d) are denoted T001-F, T101-F, and T010-F, where T indicates TiO_2, 001/101/010 the dominant facet, and F surface-terminating fluorine. Surface atomic structure and electronic structure: (e) schematic of atomic structure of {1 0 1}, {0 0 1}, and {0 1 0} faces; (f) UV/Vis absorption spectra of T001, T101, and T010; (g) valence-band XP spectra of T001, T101, and T010; and (h) determined valence-band and conduction-band edges of T001, T101, and T010. Reprinted from ref. [39].

solutions with mass concentrations of 0.15–0.80%, in an autoclave (see Table 1) [78]. Based on the analysis of surface morphologies of Ti plates after the hydrothermal treatment at 180 °C for 12 h in aqueous HF solutions with various concentrations they observed that if the HF concentration was maintained at 0.10%, homogeneously dispersed multi-facet microspheres with sizes of ca. 1–2 μm were achieved. The spheres consisted of anatase single crystals, looking like truncated bipyramids with (0 0 1) facets exposed outside. When the HF concentration increased to 0.15% and 0.20%, highly truncated bipyramids appeared on the Ti plates except for the multi-facet microspheres. It can be seen clearly that each truncated bipyramid possesses two parallel (0 0 1) facets and

eight (1 0 1) facets. When the HF concentration further increased to a value beyond 0.40%, most of the truncated bipyramids interlocked with each other and several defects on the (0 0 1) facet can be discerned. With increasing HF concentrations from 0.15% to 0.40%, the average size of truncated bipyramids increased almost linearly from 2.4 to 11.8 μm. Further increasing the HF concentration to 0.80% resulted in truncated bipyramids with an average size of ca. 13.6 μm. The fraction of (0 0 1) facets increased from 15% to 40% with increasing HF concentrations from 0.15% to 0.30%, which reached at 49% when 0.80% HF was used [78]. They found that photoactivity of the anatase crystals in degradation of rhodamine B in water increased with decreasing size and increasing fractions of (0 0 1) facets [78].

Anatase TiO_2 crystals with coexisting two types of facets (1 0 1)–(0 0 1) and (0 1 0)–(0 0 1) were successfully synthesized by $(NH_4)_2TiF_6$ acting as titanium and fluorine sources by Ye et al. [79]. They prepared four types of anatase TiO_2 samples containing different amount of (0 0 1) facets: (a) 49%:51% of (0 0 1)/(1 0 1) facets, (b) 70%:30% of (0 0 1)/(1 0 1), (c) 48%:52% of (0 0 1)/(0 1 0) facets, and (d) 64%:36% of (0 0 1):(0 1 0) facets (see Table 1) [79]. XRD results confirmed that all samples were anatase TiO_2 with the tetragonal structure and the intensity of (0 1 0) ($\theta = 25.4^o$) peak and 0 1 0/1 0 1 increase in the order of samples containing: 48% (0 0 1) and 52% (0 1 0) > 64% (0 0 1) and 36% (0 1 0) > 70% (0 0 1) and 30% (1 0 1) > 49% (0 0 1) and 51% (1 0 1) [79]. Ye et al. observed that sample with 49%:51% of (0 0 1)/(1 0 1) facets possessed about 8 and 4 times higher photocatalytic oxidation and reduction activity respectively, in comparison to sample containing 48%:52% of (0 0 1)/(0 1 0) facets. Sample having 70%:30% of (0 0 1)/(1 0 1) (BET surface area: 10.4 m^2/g) also displayed higher photocatalytic oxidation and reduction activity than sample 64%:36% of (0 0 1)/(0 1 0) (BET surface area: 8.6 m^2/g). It could be concluded the photocatalytic activity was repressed when (1 0 1) facets were replaced by (0 1 0) facets [79]. To explore the electron transfer paths between (0 0 1) and (0 1 0) facets or (0 0 1) and (1 0 1) facets, Ag deposition reaction was investigated. Ag particles of a few nanometers in size were mainly observed on (1 0 1) facets at 70%:30% of (0 0 1)/(1 0 1) sample. However, in the case of (0 0 1)/(0 1 0) sample, Ag nanoparticles were heavily observed on the (0 0 1) facets. This proves that most photoinduced electron transfer to (1 0 1) facets for (1 0 1)–(0 0 1) and (0 0 1) facets for (0 1 0)–(0 0 1) samples [79]. From the CB and VB energy level analyses and Ag deposition experiment, the relative CB and VB position of obtained samples were suggested by Ye *at al.* (Fig. 11) [79]. For (1 0 1)–(0 0 1) samples (Fig. 11a), photoinduced charge transfer tendency can be found. Under UV light irradiation, the photoinduced electrons transfer to (1 0 1) facets and holes to (0 0 1) facets. Then, photocatalytic oxidation and reduction takes place on (0 0 1) and (1 0 1) facets, respectively (Fig. 11c). However, when (1 0 1) facets were replaced by (0 1 0) facets, the transfer scenario changed. The most electrons and holes transfer to (0 0 1) facets together and do not separate anymore under UV light irradiation (Fig. 11b). The photocatalytic oxidation and reduction are supposed occurring on (0 0 1) or (0 1 0) facets synchronously (Fig. 11d). The replacement of (1 0 1) by (0 1 0) facets is thus to inhibit the photocatalytic activity of anatase TiO_2. Photocatalytic results obtained by Ye et al. showed that the replacement of (1 0 1) (50% surface undercoordinated Ti5c atoms) by (0 1 0) (100% surface undercoordinated Ti5c atoms) facets inhibits the photocatalytic activity of anatase TiO_2 for •OH production. It indicated that the separation efficiency of photogenerated electron–hole is more important than the adsorption condition of H_2O for •OH production [79].

To find the answer how does the decahedral shape itself affect the photocatalytic activity, Ohtani et al. investigated photocatalytic activities together with physical and structural properties of 35 commercial titania powders to find the predominant property

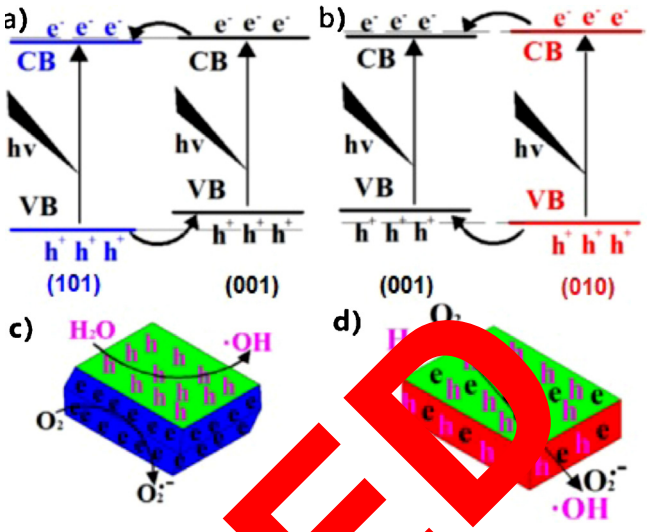

Fig. 11. Electronic band structure and charge carrier distribution: (a) electronic band structures of (1 0 1)–(0 0 1); (b) electronic band structures of (0 1 0)–(0 0 1); (c) electrons and holes distributing of (1 0 1); and (d) electrons and holes distributing of (0 1 0)–(0 0 1). Reprinted from ref. [79].

(property) determining the activity of a given reaction system [80]. They found that standardized photocatalytic activities for five kinds of reactions were fairly well reproduced by a linear combination of five kinds of physical and structural properties of photocatalysts, i.e., specific surface area, density of crystalline defects, primary particle size, secondary particle size and existence of anatase and rutile phases. It was suggested that high levels of photocatalytic activity of decahedral nanoparticles could not be reproduced by the correlation equations derived in the above-mentioned multivariable analysis [80], i.e., another property, such as "shape" may affect the photocatalytic activities [81].

In general, the photocatalytic performance of TiO_2 highly depends on the shape, size and, particularly, dominant facets. Theoretical and experimental studies have suggested that anatase TiO_2 with (0 0 1) facets are highly active. Since Yang et al. reported the preparation of anatase TiO_2 with exposed (0 0 1) facets [71], much attention has been paid on the development of TiO_2 with active facets of higher percentage. Based on this method, the percentage of TiO_2 exposed (0 0 1) facets was increased to 89%, using hydrofluoric acid as the shape capping agent [49].

Until now, anatase TiO_2 single crystals with exposed (0 0 1) facets have been successfully achieved from different raw materials, such as titanium fluoride, titanium chloride, titanium tetrabutoxide, titanium tetraisopropoxide, and so. However, these materials are usually toxic, high hydrolytic reactive and expensive, making them difficult to control the reaction processes and use in large scale. Therefore, materials with properties of no-toxicity, low-cost and stability, which is the key factor for the practical application of this advanced material, are highly required for the large scale production of anatase TiO_2 single crystals with exposed (0 0 1) facets [82].

5. Effect of metal and nonmetal doping of TiO_2 with exposed facets for enhanced visible-light photocatalytic activity

It is known that the photocatalytic activity of TiO_2 is strongly dependent on its phase structures, crystallinity, and surface energy, and the average (0 0 1) surface energy of anatase TiO_2 has been demonstrated to be higher than that of (1 0 0) and (1 0 1) surface. However, anatase TiO_2 sheets can only absorb UV light with a

wavelength of no longer than 387 nm due to the large band gap of 3.2 eV. To make a better use of the solar illumination, one approach to extend the absorption band edge of TiO_2 from the ultraviolet to the visible-light region several works reported fabrication of metal and nonmetal-doped anatase TiO_2 sheets with exposed facets, but it is still challenging to incorporate dopants into anatase TiO_2 sheets with dominant facets [70,83–91]. This is because well-faceted anatase TiO_2 sheets usually have very high crystallinity, making it difficult or nearly impossible to incorporate dopants into them by mild post-treatment, and at the same time the addition of dopant precursors in the reaction medium may inevitably influence the nucleation and growth of anatase TiO_2 sheets so that no desirable TiO_2 sheets could be synthesized [86].

Fluorine-modification on the TiO_2 surface displays the promoting effect of the photocatalytic activity. Yu et al. demonstrate that the fluorine-modification enhances the selectivity in photodegradation of organic dyes due to the different adsorption sites [92]. As reported by Yang et al. the presence of fluoride ions in the hydrothermal fluid can induce the crystal growth of anatase TiO_2 toward exposed (0 0 1) facets [71]. Li et al. reported the F^- modification on exposed (0 0 1) and (1 0 1) facets of anatase TiO_2, which exhibited different photocatalytic performances in rhodamine B and methylene orange degradation [70]. Fluorine-doped anatase TiO_2 nanosheets dominant with (0 0 1) facet exposed were synthesized *via* a hydrothermal route (see Table 4). As it was said before the photoelectrons selectively migrated toward (1 0 1) facets while photo-induced holes tended to (0 0 1) facets. Thus, more •OH radicals would be generated on (0 0 1) facets while more $•O_2^-$ radicals might be formed on (1 0 1) facets, which could sufficiently account for the higher activity of TiO_2 with dominant (0 0 1) than (1 0 1) facets in the photocatalytic degradation of rhodamine B o… the exposed (0 0 1) facets favoring the formation of •OH ra…ars. Meanwhile, it could also account for the higher activity of TiO_2 …th dominant (1 0 1) than (0 0 1)facets in the photocatalytic degr… tion of methylene orange since the dominant (1… …ts favo… the formation of $•O_2^-$ radicals as active s…es fo…ethyle… orange oxidation [70]. To summarize, Li e…stated …t F^- mod… ification promoted the rhodamine B d…grad… …1) and (1 0 1) facets. Meanwhile, F^- m…ication …enhanced the methylene orange degradation …01) facet b…ecreased it on (1 0 1) facet. Based on the s…tiv…igration of p…otoinduced electrons and holes, the enhanced carri… …eparation by the modification of fluorine wou…ncrease •OH …als generated from more holes, but the tr… of electrons by ads…bed fluorine would inhibit the formatio… $•O_2^-$ …cals. Different effects of adsorbed fluorine to the forma… of…ive spec…s contributed to the selective photodegradation o…anic d… [70] (Table 5).

Liu et al… …d sulf… p…anatase TiO_2 sheets with well faceted (…1) an… 001) b… …ng crystalline TiS_2 as titanium source… hydrot…mal route (see Table 4) [85]. They obtained relatively …if… …i… …with a particle size of ca. 1 μm. From the symme… of anatase TiO_2, two flat and square surfaces and eight isoscele… …pezoidal surfaces in the well faceted particles can be attribute… (0 0 1) and (1 0 1) facets of the anatase TiO_2 crystal [85]. The photocatalytic activity of the synthesized S-doped anatase TiO_2 sheets was estimated by detecting the generation of photocatalytic active species •OH radicals under the irradiation of UV–visible light (220–770 nm) and visible light (420–770 nm). •OH radicals react with terephthalic acid (TA) in basic solution and generate 2-hydroxyl terephthalic acid (TAOH), which emits a unique fluorescence signal with the peak at 426 nm [85]. Fluorescence spectra associated with TAOH are generated upon UV–VIS irradiation of the sulfur doped anatase TiO_2 sheets suspended in TA solution, indicating that the changed surface structure is still active in transferring photoinduced charge carriers to reactants such as surface adsorbed water and hydroxyl groups. Liu et al. observed that the nearly linear relationship between fluorescence intensity and irradiation time confirms the stability of sulfur doped anatase TiO_2 sheets synthesized. Importantly, a certain amount of •OH radicals is still generated when only visible light was employed to excite sulfur doped anatase TiO_2 sheets, suggesting that sulfur doping can indeed realize the visible light photoactivity of anatase TiO_2 sheets with preferential (0 0 1) facets. The relatively low content of •OH radicals under visible light irradiation may be due to the large particle size and low visible light absorbance of the anatase TiO_2 sheets [85]. Based on comparison of photodegradation of rhodamine B with sulfur doped anatase TiO_2 sheets in contrast to undoped anatase TiO_2 sheets it was concluded that under UV–visible light irradiation, sul… …leads to a marginal increase in the photodegradation …e. Sulfur …d anatase TiO_2 sheets show a superior visible lig… …hotodegrad…on rate of RhB to undoped anatase TiO_2 she…s [85].

Carbon self-doped TiO… …eets (CTS) …h ex…ed (0 0 1) facets obtained by hydrother… treatm…t of ti… carbide (TiC) in a HNO_3-HF mixed aqu… solu… were repo…ted by Yu et al. [93]. Titanium carbate …as u… …a precu… of TiO_2 and a source of C, which was …doped … the l…e of anatase sheets. They observed th… presence …the reaction system strongly affected t…o…logy of the …oped TiO_2 sample. Before hydrothermal treatmen… pristine TiC appeared as large, smooth and com…d particles. …r hydrothermal treatment in HNO_3-HF …d solution, the int…sectional sheets are observed. The first-…nciple calculations indicate that fluorine ions can greatly reduce …e surface e…y of (0 0 1) facets, making them more stable than …(1 0 1) fac… The average grain size of CTS is ca. 500 nm with a t…ess …a. 120 nm and percentage of ca. 58% (0 0 1) facets calcula… …y the previously reported method [93]. The XPS analy…is showed that C in CTS exists in two forms: carbons substituting …r atoms and interstitial carbon atoms present in TiO_2. The C-doped TiO_2 samples exhibited an enhanced absorption in the whole visible light region and a red shift in the absorption edges. The first-principle DFT calculations further confirm the red shift of the absorption edges and the narrowness of the band gap of the C-doped TiO_2 [93]. The photocatalytic studies in model reaction of methylene blue (MB) degradation showed that these sheets exhibited much higher photocatalytic activity than that of the C-doped TiO_2 nanoparticles due to the presence of exposed (0 0 1) facets [93]. From comparison of photocatalytic activities of the CTS, TNS and P25 samples Yu et al. observed that the C-doped TiO_2 sheets with exposed (0 0 1) facets exhibited much higher photocatalytic activity than the pure TiO_2nanosheets due to better crystallinity and higher percentage of the exposed (0 0 1) facets. Based on obtained data Yu et al. summarized the self-sensitized degradation mechanism of MB on pure TiO_2 under visible light illumination. MB molecules are excited in the first step of reaction, and next, the photoexcited electrons are transferred to the conduction band of TiO_2. Subsequently, the injected electrons can be further transferred to the adsorbed O_2 on the surface of TiO_2 to form initially the superoxide radical anions, $•O_2^-$ next, protonation yields the HOO• radicals, which after trapping electrons combine to produce H_2O_2, and finally, •OH radicals. The produced •OH radicals are responsible for the degradation of MB molecules [93].

Zhou et al. synthesized nanometre-sized nitrogen doped anatase TiO_2 sheets with dominant (0 0 1) facets (denoted as NT-001) by solvothermal treatment of TiN in acidic $NaBF_4$ solution [86]. Based on SEM analysis it can be seen that the TiO_2 products are uniform in size and appear as nanosheets. The width of their top surface is ca. 170–185 nm and the thickness of TiO_2 nanosheets is ca. 25–35 nm. The percentages of (0 0 1) facets are estimated to be 70% [86]. The presence of nitrogen in samples was confirmed by XPS analysis. Two bonding states of nitrogen species are evidenced by

Table 4
Summary of SEM/TEM images, particle size, synthesis conditions and photocatalytic activity of anatase doped-TiO_2 crystals with exposed crystal facets.

SEM/TEM image	Particle/crystal or grain size	Doping moiety	TiO_2 precursor	Synthesis parameters	Model compound and its initial concentration	Experimental conditions	Photocatalytic acitivity	Ref
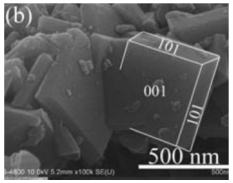	Grain size: 500 nm with 120 nm thickness	C	TiC	Precursor: 1.2 g TiC, Morphology controlling agent: 60 ml of 0.35 M HF and 0.75 M HNO_3, Procedure: hydrothermal process, 180 °C, 16 h Drying: 100 °C, 6 h.	2×10^{-5} M methy[illegible]lue $5 \times$ [illegible] M ter[illegible]hthalic	[illegible] TiO_2 [illegible] ml of MB, Ir[illegible]ource: 350 W Xen[illegible]mp (λ = 420 nm), 120 min 0.1 g TiO_2 in aqueous solution of terephthalic acid and 2×10^{-3} M NaOH.	C-TiO_2 has shown higher photocatalytic activity than P25 Fluorescence signal intensity of the 2-hydroxy terephthalic acid was highest for C-TiO_2 nanosheets	[85]
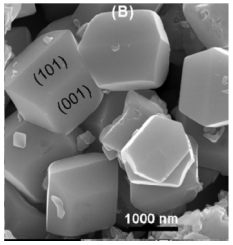	Size: 1 μm	S	TiS_2	Precursor: [illegible] Morphology [illegible]ntrolling agent: 20 ml [illegible]50 [illegible]) [illegible]Procedure [illegible]hermal p[illegible]ss, 180 [illegible]12 h, Dry[illegible]under re[illegible]d pressure [illegible]om [illegible]	rhodamine B (2×10^{-5} mol dm^{-3}) terephthalic acid (3 mM)	50 mg TiO_2 in 100 ml of RhB, Irradiation source: 300 W xenon lamp UV–VIS (220–770 nm) and VIS (420–770 nm) for 120 min 5 mg TiO_2 in 80 ml aqueous solution containing 0.01 M NaOH and 3 mM terephthalic acid.	Under UV light irradiation S-TiO_2 showed slight increase in comparison with undoped TiO_2. Under visible light S-TiO_2 exhibited significant increase in the photodegradation rate of RhB Fluorescence signal intensity of the 2-hydroxy terephthalic acid was more than: 8000 a.u. under UV light and 600 a.u. under Vis light.	[86]
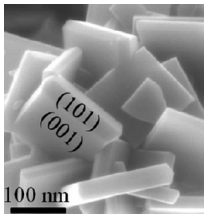	Crystal [illegible] 170–[illegible]m; thi[illegible]ss 2[illegible]m		TiN	TiO_2 and dopant precursors: TiN, Morphology controlling agent: $NaBF_4$, Procedure: solvothermal treatment, Calcination: 500 °C, 2 h.	Methylene blue	Visible light irradiation	Decolorization ratios of MB are 35% and 85% for N-P25 and the annealed NT-001, respectively.	[87]

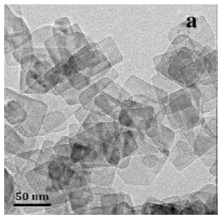	Size: 15 nm	F	$Ti(OC_4H_9)_4$	Precursor: $Ti(OC_4H_9)_4$, Dopant precursor: 30 ml 2% HF Morphology controlling agent: 3 ml 40 wt% HF, Procedure: hydrothermal process, 180 °C, 24 h	Rhodamine B or methyl orang… (2×10^{-5} m… m^3)	100… quartz reacto… …ining 0.02… …otocataly… …d 50 ml …ion … …B or MO, Irr… …source: 8 W UV-la…ps (λ = 365 nm).	F-modified TiO_2 with exposed {0 0 1} facet has shown higher photocatalytic activity in comparison with pure TiO_2 for RhB and lower activity in the case of MO	[70]
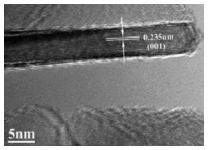	Crystal size: 22.9 nm	N/S	$Ti(OC_4H_9)_4$	Precursors: $Ti(OC_4H_9)_4$, Dopant precursor: thiourea, Morphology controlling agent: 3 ml 40 wt% HF… …edure: hydrother… 180 °C, 24 h… …ving… reduced pre…e, 80 °… 8 h, Calcinatio… …0… …2 h.	4-chlorophenol 1×10^{-4} … dm^{-3}	Irradiation source: 350 W xenon lamp, UV light ($\lambda \leq 400$ nm)	Photocatalytic activity was 3 times higher than pure TiO_2 and more than 2 times in comparison with P25.	[88]
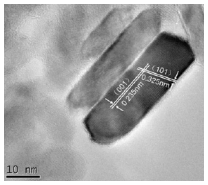	Nanosized crystallite	N/S	TiF_4	…opant …ecursor: th…urea, …lvent: 400 ml …utanol, Procedure: so…t-thermal process, 180 °C, 24 h, Calcination: 300, 400, 500 °C, 2 h.	Methylene blue 1 mg/ml	Irradiation source: 300 W xenon lamp, Vis light ($\lambda > 400$ nm) Irradiation time: 30 min	F-TiO_2 with high percentage of {0 0 1} facets exhibited faster degradation effect on MB than pure TiO_2 prepared by the same condition and commercial P25.	[89]
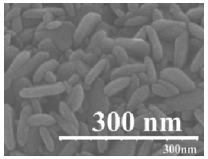	Size: 80 nm	N	Ti…	Precursor: TiN Morphology controlling agent: HNO_3-HF solution	Methanol	No data	Linear relationship between fluorescence intensity and irradiation time indicates that the amount of •OH generated on the TiO_2 surface is proportional to the irradiation time during the photocatalytic process	[95]

Table 4 (*Continued*)

SEM/TEM image	Particle/crystal or grain size	Doping moiety	TiO_2 precursor	Synthesis parameters	Model comp… and its in… concer…	…rimenta… …ditions	Photocatalytic acitivity	Ref
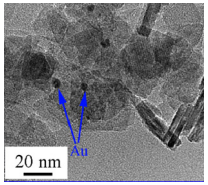	Crystal size: 15.9 nm	Au	$Ti(OC_4H_9)_4$	Precursor: $Ti(OC_4H_9)_4$, Morphology controlling agent: 3 ml 47 wt% HF, Procedure: hydrothermal process, 180 °C, 24 h, Drying: 80… …nant precursor: … H_2AuCl_4	Rhodamine B 2×10^{-5} M	80 mg TiO_2 in 80 ml RhB, Irradiation source: 300 W xenon lamp with cut-off filter (420 nm).	Au-TiO_2 has shown higher photocatalytic activity ($k = 3\ h^{-1}$) than pure TiO_2 with exposed {0 0 1} facet ($k = 0.54\ h^{-1}$).	[100]
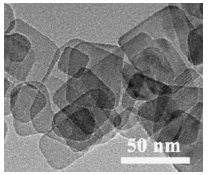	Crystalline size: 15 nm	Pt	$Ti(OC_4H_9)$…	Precu…rs: $Ti(OC_4$… Mo… …ntrol…ng …wt% HF, …cedure: hydrothermal …ss, 180 °C, 24 h, D… …80 °C, 6 h, Pt prec…sor: H_2PtCl_6, impregnation method (2 wt% ratio of Pt/TiO_2).	Ethanol Coumarin 1×10^{-3} M	20 mg TiO_2 in 80 ml of ethanol (20 ml) and water (60 ml), irradiation source: 350 W xenon arc lamp. 20 mg TiO_2 in 80 ml of ethanol (20 ml) and coumarin (60 ml), UV irradiation for 1 h.	Pt-TiO_2 nanosheets with exposed {0 0 1} facet has reached the highest photocatalytic activity 333.5 μmol h^{-1}, higher than Pt-P25 (223.4 μmol h^{-1}) and undoped TiO_2 (3 μmol h^{-1}). Pt-TiO_2 exhibited highest fluorescence signal intensity of 7-hydroxycoumarin.	[101]

Table 5
Physicochemical properties of the samples prepared at different experimental conditions. *Reprinted from ref.* [94].

No.	Experimental conditions	Phase[a]	S_{BET} (m^2/g)	C/Ti[b]	Band gap (eV)	RC[c]
CTS	TiC + HF + HNO_3 180 °C, 16 h	A	12	0.175	2.80	2.3
TNS	$Ti(OBu)_4$ + HF 180 °C, 24 h	A	86	0	3.18	1

[a] A denote anatase.
[b] C/Ti denotes the atomic ratio of doped carbon to titanium in the C-doped TiO_2 samples.
[c] RC denotes the relative anatase crystallinity calculated using the {1 0 1} diffraction peak of anatase and TNS as a reference sample.

the bimodal peaks at 398.3 and 401.3 eV. The former is attributed to the incorporated nitrogen dopant in titania in the form of Ti–O–N linkages as the interstitial nitrogen, and the latter probably originates from surface adsorbed or contaminated nitrogen species. The amount of N dopant is ca. 1.02 at%. Photocatalytic activity of NT-001 and N-P25 was measured during of the decolorization of MB dye under visible light. The decolorization ratios of MB are 35% and 85% for N-P25 and the annealed NT-001, respectively [86].

Nitrogen self-doped TiO_2 nanosheets (NTNs) with exposed (0 0 1) facets was also prepared by Xiang et al. by a solvothermal strategy in a HNO_3–HF ethanol solution using titanium nitride (TiN) as a precursor of TiO_2 and a source of N [94]. The transmission electron microscopy analysis confirms that this sample is composed of well-defined sheets having a rectangular shape with an average side size of about 80 nm. The UV–Vis diffuse reflectance spectra of the NTNs sample and P25 showed that NTNs exhibit a greatly enhanced visible-light absorption shoulder around 400–550 nm, which is consistent with yellow color characteristic of the nitrogen doped samples [94]. Xiang et al. confirmed that the formation mechanism of nanosized anatase TiO_2 sheets with dominant (0 0 1) facets could be explained by capping of fluorine ions and [illegible] in this reaction system. The first principle calculations indica[illegible] fluorine ions can greatly reduce the surface energy of high-re[illegible]ve (0 0 1) facets and thus hinder the crystal growth along the (0[illegible] axis, leading to the truncation of octahedron to [illegible]cahed[illegible] with dominant (0 0 1) facets. Moreover, th[illegible]e of [illegible]anol as reaction medium plays an important rol[illegible]ontrol[illegible]r the syn[illegible]thesis of TiO_2 nanosheets with domin[illegible]nt ([illegible]) [illegible]an be ascribed to the fact that alcohol [illegible]d as a [illegible]ing agent, can hinder the growth of the anatase [illegible] single crys[illegible]ecause of its specific binding with the TiO_2 s[illegible]ce[illegible] the Ti–O–C [illegible]d [94]. The visible-light photocatalytic activity of n[illegible]en NTNs and nitrogen doped TiO_2 microcrystalli[illegible] (NTMs) was e[illegible]ated by detection of •OH and photocatalyti[illegible]drogen production[illegible] methanol aqueous solutions by measu[illegible]ent of[illegible]e fluorescence spectra of visible light irradiated tere[illegible]ali[illegible]id solu[illegible]ion/NTNs system. The linear relationship betwe[illegible]luoresc[illegible]e intensity and irradiation time indica[illegible] the a[illegible]nt[illegible] •OH generated on the TiO_2 surface i[illegible]sporti[illegible]al to the [illegible]iation time during the photocatalytic [illegible]ess, c[illegible]rming the stability of the NTNs. Importantly, the rate [illegible]ormation of •OH radicals on NTNs is much high[illegible]an that on NTMs, indicating that the specific surface area play[illegible] important role in the photocatalytic reaction due to the large[illegible]mount of surface active sites [94]. Comparison of photocatalytic H_2-production rates obtained for the NTNs and NTMs loaded with 0.5 wt% Pt under visible-light irradiation using methanol as a scavenger showed that the H_2-production rate of the NTNs (865 μmol h^{-1} g^{-1} with a 3.7 apparent quantum efficiency at 420 nm) is much higher (4.1 times) than that of the NTMs (211 μmol h^{-1} g^{-1}) [94].

Xiang et al. prepared nitrogen and sulfur co-doped TiO_2 nanosheets with exposed (0 0 1) facets (N–S–TiO_2) by a simple mixing-calcination method using the hydrothermally prepared TiO_2 nanosheets powder as a precursor and thiourea as a dopant [87]. A comparison of the N–S–TiO_2 samples with pure TiO_2 show two prominent absorption features: (a) the appearance of new absorption shoulders around 380–500 nm, and (b) a significant enhancement of absorbance in the ran[illegible] of 550–750 nm. The first-principle DFT calculations con[illegible] the N and S co-dopants can induce the formati[illegible] new e[illegible]y levels in the band gap, which results in the v[illegible] light resp[illegible]e of N–S–TiO_2 nanosheets. The XPS analy[illegible]s sho[illegible]that nitr[illegible]en and sulfur atoms are incorporated i[illegible]he latti[illegible]TiO[illegible] interstitial N-doping and cationic sul[illegible]tution-[illegible]pe S-[illegible] respectively [87]. It was observed th[illegible]S co[illegible]ped TiO_2 [illegible]anosheets exhibited much higher pho[illegible]cat[illegible]tivity t[illegible]n pure TiO_2 nanosheets and N,S co-do[illegible]TiO_2 i[illegible]articl[illegible]ecause of their enhanced visible-light[illegible]rption and[illegible]posed (0 0 1) facets [87]. The XPS analy[illegible]sh[illegible]d that nitro[illegible]n and sulfur atoms are incorporated into the latt[illegible]f TiO_2 *via* interstitial N-doping and cationic subst[illegible]ion-type S-[illegible]ing, respectively [87]. The visible-light i[illegible]ced photocatalytic a[illegible]ivity of the doped samples was evaluated [illegible] degradation of 4-chlorophenol in aqueous solution. Activity of N–S–TiO_2 [illegible]osheets was higher than that of pure (un-doped) nanoshe[illegible]due to the enhanced visible-light absorbance. The ob[illegible]d en[illegible]icement in the visible-light photocatalytic activity is ma[illegible]ue to the synergetic effects of two factors: (i) the red-shift of absorption edges and intense absorption in the visible-light [illegible] of the doped samples, and (ii) the exposure of highly reactive (0 0 1) facets of nanosheets [87]. Surprisingly, pure TiO_2 nanosheets also showed the visible light photocatalytic activity for the degradation of 4-CP due to substrate-surface complexation between TiO_2 and 4-CP, which extends the absorption of titania to visible light region through ligand to titanium charge transfer [87].

Shi et al. obtained nitrogen/sulfur co-doped anatase TiO_2 nanocrystals with a high specific surface area and a high percentage of (0 0 1) facets by a solvent-thermal process followed by the calcination with thiourea at an optimum heat treatment temperature [88]. The morphology control technique and the anion-doping technique were combined to further enhance the visible-light-activated photocatalytic performance of anatase TiO_2 single crystals with exposed (0 0 1) facets. By the adoption of the solvent-thermal process, nanosized anatase TiO_2 crystals with a high percentage of (0 0 1) facets were obtained which largely enhanced their specific surface areas. It had been demonstrated that anion co-doping may provide better visible-light absorption and photocatalytic performance than TiO_2 or singly doped TiO_2 with either dopant. To further enhance their visible-light activity, a nitrogen/sulfur co-doping was introduced into this material system by a proper heat treatment with thiourea to replace a small portion of oxygen atoms in the anatase lattice while preserving the exposed (0 0 1) facet morphology [88]. XPS analysis results, confirmed that nitrogen/sulfur co-doping was introduced after calcinations with thiourea in the structure of TiO_2 nanocrystals with a high percentage of (0 0 1) facets. The N 1s peak at 397.3 eV is associated with Ti-N bonding which clearly demonstrated that nitrogen atoms were doped into the anatase lattice and replaced a small portion of oxygen atoms during the synthesis process, whilethe N 1s peaks at 398.5 and 399.8 eV represent some organic impurities or chemisorb N_2 on the sample surface. The doped N accounted for about 10.5% of the total N; thus, the doped N/Ti atomic ratio was determined at approximately 8.9%. The S 2p peak at 164.0 eV corresponded to the Ti-S

bonding, while the S 2p peak at 168.7 eV corresponded to the surface S atoms adsorbed as SO_2 molecules. The doped S accounted for about 34.8% of the total S; thus, the doped S/Ti atomic ratio was determined at approximately 1.0% [88]. The visible-light photocatalytic activities of the N-TiO_2 nanocrystals were evaluated) by photocatalytic degradation of MB and inactivation of *E. coli* under visible-light illumination ($\lambda > 400$ nm). The nitrogen doped sample (calcined at 300 °C), demonstrated a much faster degradation effect on MB under visible-light illumination than both P25 TiO_2 and pure TiO_2. Within just 5 min, most of the MB in the solution was degraded, and the residual MB percentage dropped to just approximately 14%. After a 30-min treatment, the residual MB percentage was near zero, suggesting a complete degradation of MB [88]. The same sample demonstrated also a much better photocatalytic inactivation effect on *E. coli* under visible-light illumination than P25 and pure TiO_2. The survival ratio of *E. coli* showed a continuous decreasing trend with the increase of visible-light illumination time. After a 2-h treatment, the survival ratio of *E. coli* dropped to around 50% [88].

Noble metals have attracted significant interest due to their unique electronic, optical, and magnetic properties. It is reported that noble metals (such as Au, Ag, and Pt) can strongly absorb visible light due to their surface plasmon resonance (SPR) effect [95,96]. Thereafter, the noble mental nanoparticles deposited on TiO_2 were considered as an approach to extend the spectral response of TiO_2 to visible light. The photocatalytic activities of noble metal semiconductor nanocomposites are strongly related to their physical characteristics, such as size and shape. It was shown for Au nanoparticles, that their catalytic activities are very sensitive to their sizes. Gold nanoparticles less than 5 nm in size are very active catalysts. Large gold nanoparticles supported on metal oxide o bon with diameter of about 50 nm and more exhibit photocata activity for hydrogen production, environmental pollution cont low-temperature catalytic combustion and reduction of nitroge oxides [97].

Zhu et al. prepared visible-light-driven plasm pho atalyst Au/TiO_2 nanosheets with a high percentage of sed (facets by hydrothermal treatment of tetrabutylti nat acid, followed by the sulfide-mediate olyol re ion process [98]. Zhu et al. prepared a series of nanosheet ded with different amount of Au (Au wt% = 1. d 2.0) [98].

From diffuse reflectance spectra of the e TiO_2-001 and the Au-modified TiO_2-001 it ca apparently o ved that the Au-TiO_2-001 samples have a onger absorption the visible light region due to the SPR ct of A eposited on TiO_2 surface. The absorption peak appea t 546 nm is assigned to the characteristic SPR pea of Au particle was observed that with increasing co u, the n intensity of Au SPR peak significantl nance 98]. XPS lysis showed that that the oxidation st of Au TiO$_2$-001 are Au^0. For Au, the core lines are fixed at (and the spin orbit separations are 3.6 eV [98]. It reported that after supporting of Au NPs on the surface of TiO_2-001, the Au/TiO_2-001 photocatalysts showed much higher photocatalytic activity than the bare TiO_2-001 for the degradation of RhB in aqueous solution under visible light, and the Au1.0/TiO_2-001 photocatalyst exhibits the highest photocatalytic efficiency among all the samples [98]. Moreover, the degradation rate of RhB over Au/TiO_2-001 is much faster than that for other Au-modified photocatalysts, such as Au/P25, Au/anatase TiO_2 and Au/rutile TiO_2. Observed enhancement in the visible-light photocatalytic activity could be related due to the synergetic effects of three factors: (1) the exposure of highly reactive (0 0 1) facets for nanosheets; (2) the higher migration rate of injected electrons from photo-excited Au to (0 0 1) facet compared with the other facets; (3) the more adsorption of pollutant mo 0 1) facet with high surface energy [98]. Zhu et al. s d that u visible light irradiation, a charge carriers have be roduced by SPR effect of Au NPs on the TiO_2-001 su face. to the p ogenerated electrons with a more negati potential pare with the conduction band (CB) level o $_2$-001 he ele would transfer from an excited Au nan ticles a TiO_2 pa icle. The photocatalytic degradation o RhB d would art from holes ($^{\bullet}Au^{+}$) attack. At the sam e, the p ogene d electron injected into the conductio d of TiO_2 m pped by adsorbed oxygen to form $^{\bullet}O_2^-$ ic And then, th O_2^- radicals can further react with H^+ and the trapp lectron to produce H_2O_2 in aqueous solution. Th med H_2O_2 d be transformed into $^{\bullet}OH$ radicals by cap g an electron. Fina y, the reactants may be destroyed by th rming $^{\bullet}O_2^-$ and $^{\bullet}OH$ radicals. In addition, the adsorbed RhB m cule can be oto-excited to form RhB* radical which may also tra s an elec n to the CB of TiO_2 to form $RhB^{\bullet+}$. This photosensi ion p ess would also lead to the decomposition of RhB [98].

u et al. synthesized Pt/TiO_2nanosheets with exposed (0 0 1) d hydrothermal treatment of tetrabutyltitanate and ydrofluoric acid mixture followed by the photochemical reduction deposition of Pt nanoparticles on TiO_2 nanosheets and discussed the effect of the Pt loading content on the rates of photocatalytic hydrogen production (see details in Table 6) [99]. TiO_2 nanosheets (NS1) fabricated by hydrothermal method without Pt deposition consists of well-defined sheet-shaped structures having a rectangular outline with an average side length of ca. 50–80 nm and thickness of ca. 6 nm. HRTEM image indicates that the lattice spacing parallel to the top and bottom facets is ca. 0.235 nm, corresponding to the (0 0 1) planes of anatase TiO_2. On the basis of the TEM results, the percentage of exposed (0 0 1) facets on the TiO_2nanosheets is ca. 75%. Pt nanoparticles with average diameter of ca. 2–4 nm are clearly observed due to their high electron density and good immobilization on the surface of TiO_2 nanosheets. HRTEM image of Pt nanoparticles indicates that the lattice fringes of 0.227 nm match the crystallographic planes of Pt (1 1 1) [99]. The XPS analysis was carried out to determine chemical composition of Pt/TiO_2nanosheetsand to identify the chemical status of Pt in samples. The binding energies corresponding to Pt $4f_{7/2}$ and Pt $4f_{5/2}$

Table 6
Experimental conditions for the preparation of TiO_2/Pt samples and their photocatalytic activity in hydrogen production process. *Reprinted from ref.* [100].

Sample label	R_F	Morphology	Phase[a]	Pt weight ratio R_{Pt}	Composition	Color	Crystalline size (nm)	S_{BET} (m^2/g)	Activity (μmol h^{-1})
NS1	1	Nanosheets	A	0	TiO_2/F	White	14.9	108	3.0
NS2	1	Nanosheets	A	0.5	TiO_2/F/Pt	Light gray	15.1	101	236.6
NS3	1	Nanosheets	A	1	TiO_2/F/Pt	Light gray	15.2	96	306.5
NS4	1	Nanosheets	A	2	TiO_2/F/Pt	Gray	15.0	94	333.5
NS5	1	Nanosheets	A	4	TiO_2/F/Pt	Black	14.9	93	308.7
NS6	1	Nanosheets	A	6	TiO_2/F/Pt	Black	14.8	84	270.9
NS7	1	Nanosheets	A	2	TiO_2/F/Pt	Gray	15.1	104	185.0
P25	0	nanoparticles	A, R	2	TiO_2/Pt	Gray	30.1	41	223.4
NP	0	nanoparticles	A	2	TiO_2/Pt	Gray	12.0	105	170.2

[a] A and R denote anatase and rutile, respectively.

were 70.7 and 74.0 eV, respectively, indicative of metallic Pt. The 3.33 eV difference between the binding energies of Pt $4f_{7/2}$ and Pt $4f_{5/5}$ peaks is also characteristic of metallic Pt4f states [99]. The photocatalytic activity in hydrogen production of the Pt-TiO_2 samples grew with increasing weight ratios of Pt (R_{Pt}) from 0.5 to 2. The highest photocatalytic activity, 333.5 μmol h^{-1}, was achieved for sample loaded with 2 wt% Pt; this value exceeds that of P25. A further increase of R_{Pt} causeed a reduction of the photocatalytic activity. This is probably due to (i) partial blockage of the TiO_2 surface active sites due to excessive Pt and (ii) deterioration of the catalytic properties of metal nanoparticles due to their enlargement [99].

Yu et al. tried to explain the photocatalytic mechanism and detect the involved active species in the photocatalytic H_2 production [99]. In the presence of O_2 and in pure water, the electrons are excited from the valence band to the conduction band and then transferred to the adsorbed O_2 on the surface of TiO_2 to form the superoxide radical anions, ($O_2^{-\bullet}$), which prevent the direct recombination of electrons and holes; meanwhile, the holes react with OH^-/H_2O to produce •OH radicals. In the absence of O_2, the rates of electrons and holes recombination are faster than that of the reaction of holes and OH^-/H_2O (no •OH radicals are observed in the absence of O_2). In the presence of Pt-TiO_2 samples the production of the •OH radicals was observed which implies that Pt is an effective electron acceptor. The production of •OH radicals for Pt-TiO_2 samples can be assigned to the fact that the excited electrons from the valence band to the conduction band can migrate to Pt nanoparticles and then react with H^+ ions adsorbed to form H_2. The Pt nanoparticles on TiO_2 nanosheets produce a Schottky barrier, which facilitate the electron capture [99].

6. Perspectives and conclusions

Photocatalytic processes could be widely exploited for environmental and energy-related applications, such as photocatalytic water/air purification, hydrogen production by water splitting, low-cost solar cells, and organic synthesis, etc, as schematically shown in Fig. 12. However, from the practical point of view, photocatalytic material should be highly active, stable, recyclable, selective, and visible-light sensitive. Since Yang and co-workers [71] prepared anatase single crystals with 47% of the highly reactive (0 0 1) facets by using hydrofluoric acid (HF) as a capping agent under hydrothermal conditions, anatase TiO_2 nanosheets with dominant (0 0 1) facets seems to have ...ntial as advanced photocatalytic material [100]. Unt...oday, ana... containing up to 90% of highly reactive (0 0 1) ...ts was suc...sfully synthesized in the shape of nanosh...ets, t...ted octa...ral bipyramid or multi-facet microspher...

Both theoretical a... experim...ntal s... indicate that the (0 0 1) surface of anat... TiO_2 i... uch more reactive than the thermodynamically m...re s... 0 1) surf..., and the (0 0 1) surfaces may in fact be t... domina...urce o...tive sites for various applications (e.g. ...ocatalytic p...n of H_2). Unfortunately, most synthesiz...ana... TiO_2 crysta...s well as those naturally occurring are dominate... the thermodynamically stable (1 0 1) facets (mo...n 94%, acco... to the Wulff construction), which greatly li...s the applications ...anatase crystals in catalysis, photocata...is, and photocatalytic water splitting. Based on the literature ...view it can ...stated that the selective adhesion of specific cap... agents (...cally, fluoride) on the (0 0 1) surface of anatase is cr... for s...dizing the high-energy (0 0 1) facets. Moreover, the

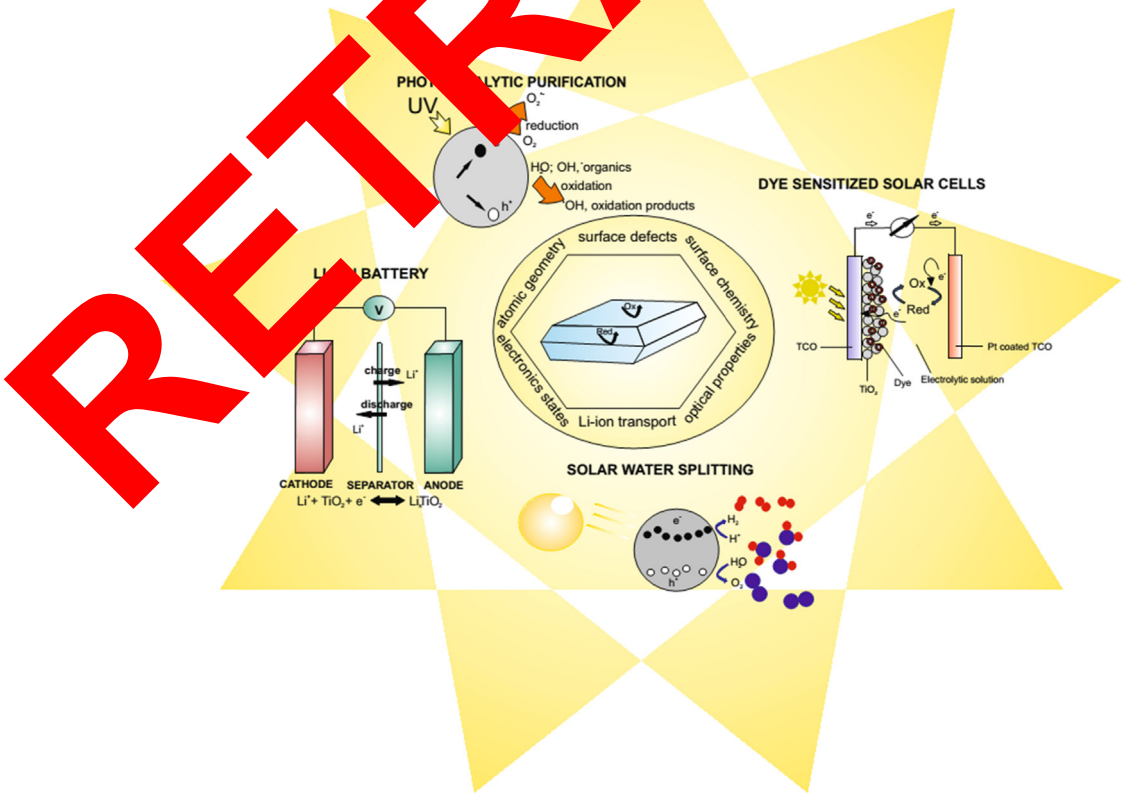

Fig. 12. Schematic diagram showing important applications of TiO_2 with high reactive facets.

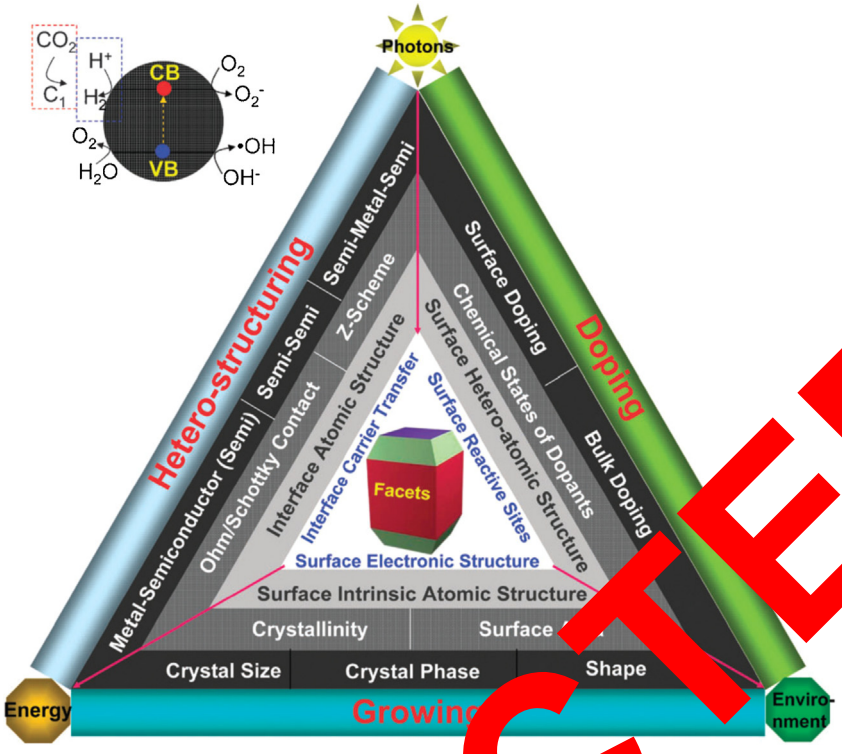

Fig. 13. Highlighted key points in growing, doping and heterostructuring of ted semicond or photocatalysts. Reprinted from ref. [61].

degree of truncation, size and organization of anatase TiO_2 s can be controlled by selecting titania precursors, capping ag solvent, and other reaction conditions. The unique geometrical a electronic properties associated with (0 0 1) facets are crucial for t charge separation and transfer occurring in photo redox processes, being a consequence of favored diss tive a rption and spatial separation of redox sites. Although nifica rogress has been achieved in the synthesis and as anatase nanosheets, further efforts ar requ in this area to obtain nanomaterials suitable for nced envi ental and energy-related applications.

Is well known, that pure TiO_2 photoca sts is suffered from weak visible-light absorptio d high recom tion rate of photoexcited electrons and h . Thus, doping and terostructuring are strategies that wil initel ntribute to the development of more efficient facete ot talysts. Doping changes the surface atomic structure of fa nd thus rs their photoreactivity. Heterostructu s effe i facial charge carrier transfer by cons ting i orable i ces with various facets from different tals. T key points related to growing, doping and heterostruc otocatalysts were summarized by Liu et al. as sh in Fig. 13 [61]. They stated that a direct consequence of contro the size, percentage of exposed (0 0 1) facets and organization of atase TiO_2 crystals is the possibility of tuning the surface and electronic properties of this material and finally affecting its potential applications [63].

Presently, anatase TiO_2 with dominant (0 0 1) face – pure, doped and surface modified – are successfully synthesized in the laboratory scale mainly *via* hydrothermal process and gas phase reaction. The visible light photocatalysts could be obtained by incorporation of sulfur, nitrogen or carbon into TiO_2 structure or by surface modification of TiO_2 sheets with noble metal nanoparticles. Even at this stage of research, there is no data regarding stability of doped photocatalysts in the subsequent reaction cycles. Based on previous experience with non-metal doped TiO_2 nanoparticles, it could be expected that doped TiO_2 can loss photoactivity during recycling ng-term storage. Additionally, the current problem synthesis of TiO_2 having dominant (0 0 1) facets is highly reaction medium during preparation and small yield TiO_2 generation. Thus, major challenges facing scientific and industrial community involved in photocatalytic research include:

- development a new synthesis strategy of decahedral TiO_2 with reduced or no fluorine containing compounds as capping agents,
- increase of synthesis efficiency and process scale-up,
- efficient doping or surface modification of decahedral TiO_2 to increase visible light utilization.

References

[1] M.R. Hoffmann, S.T. Martin, W. Choi, D.W. Bahnemann, Chem. Rev. 95 (1995) 69–96.
[2] A. Fujishima, T.N. Rao, D.A. Tryk, J. Photochem. Photobiol. C: Photochem. Rev. 1 (2000) 1–21.
[3] K. Hashimoto, H. Irie, A. Fujishima, Jap. J. Appl. Phys. 1 Regul. Papers Short Notes Rev. Papers 44 (2005) 8269.
[4] S.M. Gupta, M. Tripathi, Chin. Sci. Bull. 56 (2011) 1639–1657.
[5] K. Nakata, A. Fujishima, J. Photochem. Photobiol. C: Photochem. Rev. 13 (2012) 169–189.
[6] A.N. Banerjee, Nanotechnology, Sci. Appl. 4 (2011) 35–65.
[7] A. Zaleska, Recent Patents on Engineering 2 (2008) 157-164.
[8] A. Pérez-Larios, R. Lopez, A. Hernández-Gordillo, F. Tzompantzi, R. Gómez, L. Torres-Guerra, Fuel 100 (2012) 139–143.
[9] H.S. Kim, D. Kim, B.S. Kwak, G.B. Han, M.-H. Um, M. Kang, Chem. Eng. J. 243 (2014) 272–279.
[10] M. Niu, D. Cheng, D. Cao, Int. J. Hydrogen Energy (2012).
[11] C. Wang, Q.-Q. Hu, J.-Q. Huang, Z.-H. Deng, H.-L. Shi, L. Wu, Z.-G. Liu, Y.-G. Cao, Int. J. Hydrogen Energy 39 (2014) 1967–1971.
[12] C.W. Lai, S. Sreekantan, Int. J. Photoenergy 2013 (2013).
[13] R. Dholam, N. Patel, A. Santini, A. Miotello, Int. J. Hydrogen Energy 35 (2010) 9581–9590.
[14] G. Wang, H. Wang, Y. Ling, Y. Tang, X. Yang, R.C. Fitzmorris, C. Wang, J.Z. Zhang, Y. Li, Nano Lett. 11 (2011) 3026–3033.
[15] X. Yang, A. Wolcott, G. Wang, A. Sobo, R.C. Fitzmorris, F. Qian, J.Z. Zhang, Y. Li, Nano Lett. 9 (2009) 2331–2336.
[16] J. Choi, H. Lee, Y. Choi, S. Kim, S. Lee, S. Lee, W. Choi, J. Lee, Appl. Catal. B: Environ. 147 (2014) 8–16.
[17] M.V. Bagal, P.R. Gogate, Ultrason. Sonochem. (2013).

[18] H.U. Lee, G. Lee, J.C. Park, Y.-C. Lee, S.M. Lee, B. Son, S.Y. Park, C. Kim, S. Lee, S.C. Lee, Chem. Eng. J. 240 (2014) 91–98.
[19] S. Hu, F. Li, Z. Fan, J. Gui, Chem. Eng. J. 236 (2014) 285–292.
[20] S. Hu, F. Li, Z. Fan, Appl. Surf. Sci. 286 (2013) 228–234.
[21] M. Nischk, P. Mazierski, M. Gazda, A. Zaleska, Appl. Catal. B: Environ. 144 (2014) 674–685.
[22] P. Pichat, Appl. Catal. B: Environ. 99 (2010) 428–434.
[23] A. Zaleska, A. Hanel, M. Nischk, Recent Patents on Engineering 4 (2010) 200-216.
[24] M. Grätzel, J. Photochem. Photobiol. C: Photochem. Rev. 4 (2003) 145–153.
[25] Z. Yang, Z. Ma, D. Pan, D. Chen, F. Xu, S. Chen, Ceram. Int. (2013).
[26] I. Ding, J. Melas-Kyriazi, N.-L. Cevey-Ha, K.G. Chittibabu, S.M. Zakeeruddin, M. Grätzel, M.D. McGehee, Org. Electron. 11 (2010) 1217–1222.
[27] J.-H. Yum, R. Humphry-Baker, S.M. Zakeeruddin, M.K. Nazeeruddin, M. Grätzel, Nano Today 5 (2010) 91–98.
[28] C. Dwivedi, V. Dutta, A.K. Chandiran, M.K. Nazeeruddin, M. Grätzel, Energy Proced. 33 (2013) 223–227.
[29] A. Fujishima, X. Zhang, Comptes Rendus Chimie 9 (2006) 750–760.
[30] L. Graziani, E. Quagliarini, F. Bondioli, M. D'Orazio, Build. Environ. 71 (2014) 193–203.
[31] K.-W. Weng, Y.-P. Huang, Surf. Coat. Technol. 231 (2013) 201–204.
[32] E.I. Cedillo-González, R. Riccò, M. Montorsi, M. Montorsi, P. Falcaro, C. Siligardi, Build. Environ. 71 (2014) 7–14.
[33] K. Murugan, R. Subasri, T. Rao, A.S. Gandhi, B. Murty, Prog. Org. Coat. 76 (2013) 1756–1760.
[34] X. Zhao, W. Jin, J. Cai, J. Ye, Z. Li, Y. Ma, J. Xie, L. Qi, Adv. Funct. Mater. 21 (2011) 3554–3563.
[35] T. Ohno, K. Sarukawa, M. Matsumura, New J. Chem. 26 (2002) 1167–1170.
[36] V.M. Menéndez-Flores, M. Nakamura, T. Kida, Z. Jin, N. Murakami, T. Ohno, Appl. Catal. A: Gen. 406 (2011) 119–123.
[37] N. Sugishita, Y. Kuroda, B. Ohtani, Catal. Today 164 (2011) 391–394.
[38] N. Murakami, S. Kawakami, T. Tsubota, T. Ohno, J. Mol. Catal. A: Chem. 358 (2012) 106–111.
[39] J. Pan, G. Liu, G.Q.M. Lu, H.M. Cheng, Angew. Chem. Int. Ed. 50 (2011) 2133–2137.
[40] N. Murakami, Y. Kurihara, T. Tsubota, T. Ohno, J. Phys. Chem. C 113 (2009) 3062–3069.
[41] C. Burda, X. Chen, R. Narayanan, M.A. El-Sayed, Chem. Rev. 105 (2005) 1025–1102.
[42] N.M. Dimitrijevic, Z.V. Saponjic, B.M. Rabatic, O.G. Poluektov, T. Rajh, J. Phys. Chem. C 111 (2007) 14597–14601.
[43] J. Lowekamp, G. Rohrer, P. Morris Hotsenpiller, J. Bolt, W. Farneth, J. Phys. Chem. B 102 (1998) 7323–7327.
[44] A. Imanishi, E. Tsuji, Y. Nakato, J. Phys. Chem. C 111 (2007) 2128–2132.
[45] Y. Sun, Y. Xia, Science 298 (2002) 2176–2179.
[46] X. Peng, L. Manna, W. Yang, J. Wickham, E. Scher, A. Kadavanich, A.P. Alivisatos, Nature 404 (2000) 59–61.
[47] M. Lazzeri, A. Vittadini, A. Selloni, Phys. Rev. B 63 (2001) 155409.
[48] U. Diebold, Surf. Sci. Rep. 48 (2003) 53–229.
[49] K.Q.X.G. Han, M.S. Jin, Z.X. Xie, L.S. Zhang, J. Am. Chem. Soc. 131 (2009) 3152–3153.
[50] K. Lv, X. Li, K. Deng, J. Sun, X. Li, M. Li, Appl. Catal. B: Environ. 95 (2010) 383–392.
[51] K. Lv, Q. Xiang, J. Yu, Appl. Catal. B: Environ. 104 (2011) 275–281.
[52] K. Lv, B. Cheng, J. Yu, G. Liu, Phys. Chem. Chem. Phys. 14 (2012) 5349–5362.
[53] Z. Wang, K. Lv, G. Wang, K. Deng, D. Tang, Appl. Catal. B: Environ. 100 (2010) 378–385.
[54] Q. Xiang, K. Lv, J. Yu, Appl. Catal. B: Environ. 96 (2010) 557–564.
[55] T. Taguchi, Y. Saito, K. Sarukawa, T. Ohno, M. Matsumura, New J. Chem. 27 (2003) 1304–1306.
[56] F. Tian, Y. Zhang, J. Zhang, C. Pan, J. Phys. Chem. C 116 (2012) 7515–7519.
[57] P. Wen, H. Li, Z. Tang, Y. Feng, L. Fan, Langmuir 23 (2007) 11782–11790.
[58] Z. Zhen, H. Huang, J. Lu, X. Qian, Z. Tang, Y. Dai, Chem. A Eur. J. 17 (2011) 15025–15038.
[59] G.-B. Shan, G.P. Demopoulos, Nanotechnology 21 (2010) 025604.
[60] F. Amano, O.-O. Prieto-Mahaney, Y. Terada, T. Yasumoto, T. Shibayama, B. Ohtani, Chem. Mater. 21 (2009) 2601–2603.
[61] G. Liu, C.Y. Jimmy, G.Q.M. Lu, H.-M. Cheng, Chem. Commun. 47 (2011) 6763–6783.
[62] A. Selloni, Nat. Mater. 7 (2008) 613–615.
[63] S. Liu, J. Yu, M. Jaroniec, Chem. Mater. 23 (2011) 4085–4093.
[64] D. Zhang, G. Li, H. Wang, K.M. Chan, J.C. Yu, Cryst. Growth Des. 10 (2010) 1130–1137.
[65] J.-M. Wu, M.-L. Tang, J. Hazard. Mater. 190 (2011) 566–573.
[66] T.R. Gordon, M. Cargnello, T. Paik, F. Mangolini, R.T. Weber, P. Fornasiero, C.B. Murray, J. Am. Chem. Soc. 134 (2012) 6751–6761.
[67] H. Yu, P.C. Gibbons, K. Kelton, W.E. Buhro, J. Am. Chem. Soc. 123 (2001) 9198–9199.
[68] R. Buonsanti, V. Grillo, E. Carlino, C. Giannini, T. Kipp, R. Cingolani, P.D. Cozzoli, J. Am. Chem. Soc. 130 (2008) 11223–11233.
[69] N. Alcock, D. Brown, T. ILLSON, S. Roe, Wan, J. Chem. Soc. Dalton Trans. (1991) 873–881.
[70] X. Li, J. Zhu, H. Li, Catal. Commun. 12 (2012) 20–24.
[71] H.G. Yang, C.H. Sun, S.Z. Qiao, J. Zou, S.C. Smith, M. Cheng, G.Q. Lu, Nature 453 (2008) 638–641.
[72] N. Murakami, S. Katayama, Nakamura, botsuno, J. Phys. Chem. C 115 (2010) 419–424.
[73] H. Park, W. Choi, J. Phys. Chem. B (2004) 4093.
[74] Y. Zheng, K. Lv, Z. W, K. D, M. Li, J. Mol. Catal. A: Chem. 356 (2012) 137–143.
[75] H.G. Yang, C, S.Z. Qia, Sun, Y, S.C. Smith, J. Zou, H.M. Cheng, G.Q. Lu, J. Chem. Soc. 13 09) 4078–4083.
[76] P. Aho, Koisala, U. Tap, Brown, J. Jokiniemi, E. Kauppinen, J. Nan, Nucle (2002) 43–52.
[77] S.C.H. Liu, G. Y, G. Smith, S.C. Wang, L.Z. Lu, G.Q.H.M. Cheng, Chem. Commun. 46 (201 –757.
[7 Tang, J.-M. Wu, ard. Mater. 190 (2011) 566–573.
[L.J. Ye, L. Tian, L. Peng, L. Zan, Appl. Catal. B: Environ. 134–135 (2013) 60–65.
[O.-O. Prie ahaney, N. Murakami, R. Abe, B. Ohtani, Chem. Lett. 38 (2009) 238–239.
[B. Ohtani, otochem. Photobiol. C: Photochem. Rev. 11 (2010) 157–178.
[M. A rf. Sci. 274 (2013) 117–123.
[83] M.K. Leung, X.-Y. Lu, S.-Y. Chen, Appl. Energy (2013).
[84] J. Yu, G. Dai, Q. Xiang, M. Jaroniec, J. Mater. Chem. 21 (2011) 1049–1057.
[S.C. Liu, G. Smith, S.C. Wang, L. Lu, G.Q.H.M. Cheng, J. Colloid Interf. Sci. 349 010) 477–483.
[86] P.F. Zhou, X. Wang, H. Yu, H.Y. Fang, Chem. Commun. 48 (2012) 600–602.
[87] Y.J. Xiang, Q.M. Jaroniec, Phys. Chem. Chem. Phys. 13 (2011) 4853–4861.
[88] Y.W. Shi, W. Li, Q. Gao, S. Shang, P.J.K. Shang, Nanoscale Res. Lett. 7 (2012) 590–599.
[89] S. Zhu, S. Liang, Q. Gu, L. Xie, J. Wang, Z. Ding, P. Liu, Appl. Catal. B: Environ. 119 (2012) 146–155.
[90] J. Yu, L. Qi, M. Jaroniec, J. Phys. Chem. C 114 (2010) 13118–13125.
[91] J. Mao, L. Ye, K. Li, X. Zhang, J. Liu, T. Peng, L. Zan, Appl. Catal. B: Environ. 144 (2014) 855–862.
[92] Y.J.G. Liu, S.W.M. Jaroniec, J. Am. Chem. Soc. 132 (2010) 11914–11916.
[93] D.G. Yu, J. Xiang, Q.M. Jaroniec, J. Mater. Chem. 21 (2011) 1049–1057.
[94] Y.J. Xiang, Q. Wang, W.M. Jaroniec, Chem. Commun. 47 (2011) 6906–6908.
[95] Z.Z. Chen, X. Ke, X. Jaatinen, E.T. Xie, D. Wang, C. Guo, J. Zhao, H. Zhu, Green Chem. 12 (2010) 414–419.
[96] W.W. Sun, S. Zhang, L. Shang, M.L. Wang, Catal. Commun. 11 (2009) 290–293.
[97] K.E. Zielinska-Jurek, A. Sobczak, J.W. Lisowski, W. Ohtani, B.A. Zaleska, Appl. Catal. B: Environ. 101 (2011) 504–514.
[98] L.S. Zhu, S. Gu, Q. Xie, L. Wang, J. Ding, Z.P. Liu, Appl. Catal. B: Environ. 119–120 (2012) 146–155.
[99] Q.L. Yu, J.M. Jaroniec, J. Phys. Chem. C 114 (2010) 13118–13125.
[100] G.X.Q. Fang, W.Q.H.G. Yang, J. Phys. Chem. Lett. 2 (2011) 725–734.